6737 W. Washington St., Suite 4210 • Milwaukee, WI 53214
(p) 414-755-6296 • (f) 414-276-7704 • www.isaponline.org • isaphq@isaponline.org

Mission Statement

The International Society for Anaesthetic Pharmacology (ISAP) is a nonprofit organization with an international membership, which is dedicated to teaching and research about clinical pharmacology in anesthesia, with particular reference to anesthetic drugs.

Accreditation Information

Target Audience
This program is designed for an international audience of general anesthesiologists, pharmacological anesthesiologists, technology anesthesiologists and specialty physicians.

Objectives:
After attending this program you should be able to:

1. Understand the role of anesthesiologists in the opioid epidemic, and how to prevent long-term opioid use after surgery
2. Hear about experimental monitoring strategies and their potential to improve perioperative care
3. Comprehend how artificial intelligence can improve complex pharmacologic modeling

Practice Gaps:

- Opioid use disorder has been identified as a national epidemic. Anesthesiologists' perioperative management may influence long-term opioid use by patients.
- Reducing the health and societal consequences of opioid use requires identification of effective alternative approaches to pain management.
- Anesthetic and opioid toxicity must be minimized through improved intra-operative monitoring.
- Improved peri-operative outcomes may be achieved through discovery of novel general anesthetic drugs.
- Better pharmacokinetic and pharmacodynamic modeling is needed to improve the administration of intravenous drugs during general anesthesia.

Acknowledgement of Commercial Support

>> Masimo

>> Merck

Physicians

Accreditation Statement
This activity has been planned and implemented in accordance with the accreditation requirements and policies of the Accreditation Council for Continuing Medical Education (ACCME) through the joint providership of Amedco and the International Society for Anaesthetic Pharmacology. Amedco is accredited by the ACCME to provide continuing medical education for physicians.

Credit Designation Statement
Amedco designates this live activity for a maximum of 6.75 *AMA PRA Category 1 Credits*™. Physicians should claim only the credit commensurate with the extent of their participation in the activity.

Planning Committee
Stuart Forman, MD, PhD
Massachusetts General Hospital
Boston, MA USA

Donald Mathews, MD
University of Vermont College of Medicine
Burlington, VT USA

Faculty
T. Anthony Anderson, MD, PhD
Stanford University School of Medicine
Stanford, CA USA

Michael Avram, PhD
Northwestern University Feinberg School of Medicine
Chicago, IL USA

Jane C. Ballantyne, MD, FRCA
University of Washington
Seattle, WA USA

Brian T. Bateman, MD, MSc
Brigham and Women's Hospital
Harvard Medical School
Boston, MA USA

Stuart Forman, MD, PhD
Massachusetts General Hospital
Boston, MA USA

Tony Gin, FANZA, FRCA, MD
Chinese University of Hong Kong
Hong Kong, China

Howard B. Gutstein, MD
University of Pittsburgh
Pittsburgh, PA USA

Oluwaseun Johnson-Akeju, MD, MMSc
Massachusetts General Hospital
Harvard Medical School
Boston, MA USA

Donald Mathews, MD
University of Vermont College of Medicine
Burlington, VT USA

Gertrude Nieuwenhuijs-Moeke, MD
University of Groningen
University Medical Centre Groningen
Groningen, The Netherlands

Steven Shafer, MD
Stanford University
San Francisco, CA USA

Disclosure of Conflict of Interest

The following table of disclosure information is provided to learners and contains the relevant financial relationships that each individual in a position to control the content disclosed to Amedco. All of these relationships were treated as a conflict of interest, and have been resolved. (C7 SCS 6.1---6.2, 6.5)

All individuals in a position to control the content of CE are listed in the program book/agenda. If their name is not listed below, they disclosed that they had no relevant financial relationships.

First Name	Last Name	Company	Role
Gertrude	Nieuwenhuijs-Moeke	Baxter/ESA grant 2017	Research Grant Site Principal Investigator
Brian	Bateman	Pfizer	Research Grant Overall Principal Investigator
		Lilly	Research Grant Site Principal Investigator
		Baxalta	Research Grant Site Principal Investigator
		GSK	Research Grant Site Principal Investigator
		Pacira	Research Grant Site Principal Investigator
		Aetion	Consultant
Mohamed	Naguib	NeuroTherapia	
Sarah	Eagleman	Hospira funded the original study which I retrospectively analyzed here.	Other
Marilyn	Huestis	Intelligent Fingerprinting	Consultant
		Cannabix	Consultant
		Frederick Reiders Family Foundation	Consultant
		Evanostics, Inc.	Scientific/Medical Advisory Board Member
		Thermo Fisher	Consultant
Charles	Minto	CODAN ARGUS	Consultant
Peter	Szolovits	Acupera	Scientific/Medical Advisory Board Member
		Health Fortis	Scientific/Medical Advisory Board Member
		Vanguard Medical Technologies	Consultant
		Health Fidelity	Scientific/Medical Advisory Board Member
Ross	Kennedy	GE Healthcare	Consultant
Ken	Johnson	Medvis	Stock Shareholder
Erik	Jensen	Quantium Medical	Employee
		Quantium Medical	Stock Shareholder
Joseph	Foss	NeuroTherapia, Inc.	
Umberto	Melia	Quantium Medical	Employee
Isabel	Serra Riera	Quantium Medical	Employee
Umberto	Melia	Quantium Medical	Employee
Erik	Jensen	Quantium Medical	Employee
		Quantium Medical	Stock Shareholder
Pablo	Martinez-Vazquez	Quantium Medical, SL.	Consultant
Donald	Mathews	Masimo	Speakers Bureau
		Masimo	Consultant

Continuing Medical Education (CME) Certificate

IMPORTANT!
The online certificate site will be available from October 13th to November 13th. After that date, the site will be removed and certificates will no longer be available. If you need a CME certificate, you must complete the evaluation and certificate process prior to that date; otherwise you will forfeit your credit for the course.

To get your certificate, just go to ISAP.cmecertificateonline.com.

1. **Go to http://isap.cmecertificateonline.com**
2. **Click on the "27th Annual Meeting" link.**

Please print all pages of your certificate for your record.

Questions? Email Certificate@AmedcoEmail.com

27th Annual Meeting Agenda

07:00 – 08:00	**Breakfast & Registration**
08:00 – 08:10	**Welcome** ISAP President, David Drover, MD
08:10 – 08:15	**Introduction to the Program** Stuart Forman, MD, PhD and Donald Mathews, MD
08:15 – 9:00	**Session 1 – Anesthesiologists and the Opioid Epidemic**
08:15 – 08:35	**Opioid Epidemic Emerged and Strategies to Reverse Recent Trends** Jane C. Ballantyne, MD, FRCA
08:35 – 08:55	**Opioid-Sparing Anesthetic Strategies for Enhanced Recovery After Surgery** T. Anthony Anderson, MD, PhD
09:00 – 09:30	**Break**
09:30 – 10:30	**Session 2 – Can Perioperative Anesthesia Care Reduce Post-Operative Opioid Use?**
09:30 – 10:00	**Molecular Approaches to Reducing Opioid Tolerance** Howard B. Gutstein, MD
10:00 – 10:30	**The Correlation of Perioperative Anesthesia Approaches with Long-Term Post-Op Opioid Use** Brian T. Bateman, MD, MSc
10:30 – 11:30	**Session 3 – Improving Anesthesia With Better Monitors**
10:30 – 11:00	**New Uses for EEG Monitoring** Olewaseun Johnson-Akeju, MD, MMSc
11:00 – 11:30	**Machine Learning for PK/PD Modeling** Steven Shafer, MD
11:30 – 12:45	**Lunch, Business Meeting & Poster Session**
12:45 – 13:45	**Moderated Poster Discussion**
13:45 – 14:45	**Session 4 – New Approaches in Anesthetic Pharmacodynamics and Pharmacokinetics**
13:45 – 14:15	**Zebrafish for High-Throughput Screening and Pharmacodynamic Profiling of Novel Sedative-Hypnotic Compounds** Stuart Forman, MD, PhD
14:15 – 14:45	**Analgesia Monitors** Donald Mathews, MD
14:45 – 15:15	**Break**
15:15 – 16:15	**Session 5 – New Drug Targets in Perioperative Medicine**
15:15 – 15:45	**Potential of Volatile Anesthetics in Organ Transplantation** Gertrude Nieuwenhuijs-Moeke, MD
15:45 – 16:15	**Brain Derived Neurotrophic Factor Polymorphisms are Associated with Chronic Postsurgical Pain, Suggesting Potential Drug Targets** Tony Gin, FANZCA, FRCA, MD
16:15 – 16:55	**Keynote Speaker & Lifetime Achievement Award Winner:** Michael Avram, PhD
16:55 – 17:00	**Closing Remarks**
17:00 – 18:00	**President's Reception**

Participant Notification

All people with control of the CME content for this activity (e.g., faculty/speakers, planners, abstract reviewers, moderators, authors, co-authors and administrative staff participating) disclosed their financial relationships to Amedco as shown in the list below, which also indicates the resolution, if applicable.

We acknowledge the potential presence of limitations on information, including, but not limited to: data that represents ongoing research; interim analysis; preliminary data; unsupported opinion; or approaches to care that, while supported by some research studies, do not represent the only opinion or approach to care supported by research.

Abstract Table of Contents

Commercial Support Levels

PLATINUM PLUS SUPPORTER

Masimo®

PLATINUM SUPPORTER

MERCK

SILVER SUPPORTERS

BD

La Jolla Pharmaceutical

ENTREPRENEUER SILVER SUPPORTERS

QM Quantium Medical

MEDASENSE PAIN INTELLIGENCE

Activation of mGluR1 Mediates C1q-Dependent Microglial Phagocytosis of Glutamatergic Synapses in Alzheimer's Rodent Models

Presenting Author: Jiang Wu[1]

Co-Authors: Bihua Bie[1], Joseph F. Foss[1], Mohamed Naguib[1]

[1]Department of General Anesthesia, Anesthesiology Institute, Cleveland Clinic

Introduction: Brains of patients with Alzheimer's disease (AD) are characterized by neuroinflammation and synaptic loss. Microglia and complement appear to be involved in the synaptic and cognitive deficits seen in AD, though the mechanisms remain elusive. Our hypothesis is illustrated in **Fig. 1**.

Methods: Two types of rodent models of Alzheimer's disease, rats injected with amyloid fibrils into hippocampal CA1 and transgenic APP/PS1 mice, were used in this study. Immunostaining was applied to study the microglia phagocytosis of glutamatergic synapse, which was analyzed by confocal 3-D image. Immunoblotting was used to study the expression of C1q and other proteins. Whole-cell recording and Morris water maze were used to evaluate the synaptic and cognitive function in the rodent models.

Result: First, we noted an increased complement C1q-mediated microglial phagocytosis of the hippocampal glutamatergic synapses that resulted in synaptic and cognitive deficits in both models of AD (**Fig. 2**). We also found an increased activity of the metabotropic glutamate receptor 1 (mGluR1) in the hippocampal CA1 area. Suppression of mGluR1- protein phosphatase 2 (PP2A) signaling inhibited the dephosphorylation of FMRP and repressed the local translation of synaptic C1q mRNA (**Fig. 3**), which consequently alleviated the microglial phagocytosis of synapses in the hippocampal CA1 and restored the synaptic and cognitive function in the rodent models (**Fig. 4**). Artificial activation of mGluR1 signaling by DHPG promoted dephosphorylation of fragile X mental retardation protein (FMRP) and facilitated the local translation machinery of synaptic C1q mRNA (**Fig. 5**) —mimicking the C1q-mediated microglial phagocytosis of hippocampal glutamatergic synapses and synaptic and cognitive deficiency in the rat model (**Fig. 6**).

Conclusion: Our findings demonstrated that activation of mGluR1-PP2A signaling by amyloid fibrils induced the dephosphorylation of FMRP, which facilitated the local translation of C1q mRNA in both rodent models. This led to C1q-mediated microglial phagocytosis of hippocampal glutamatergic synapses, which contributed to the development of synaptic and cognitive deficiency in AD.

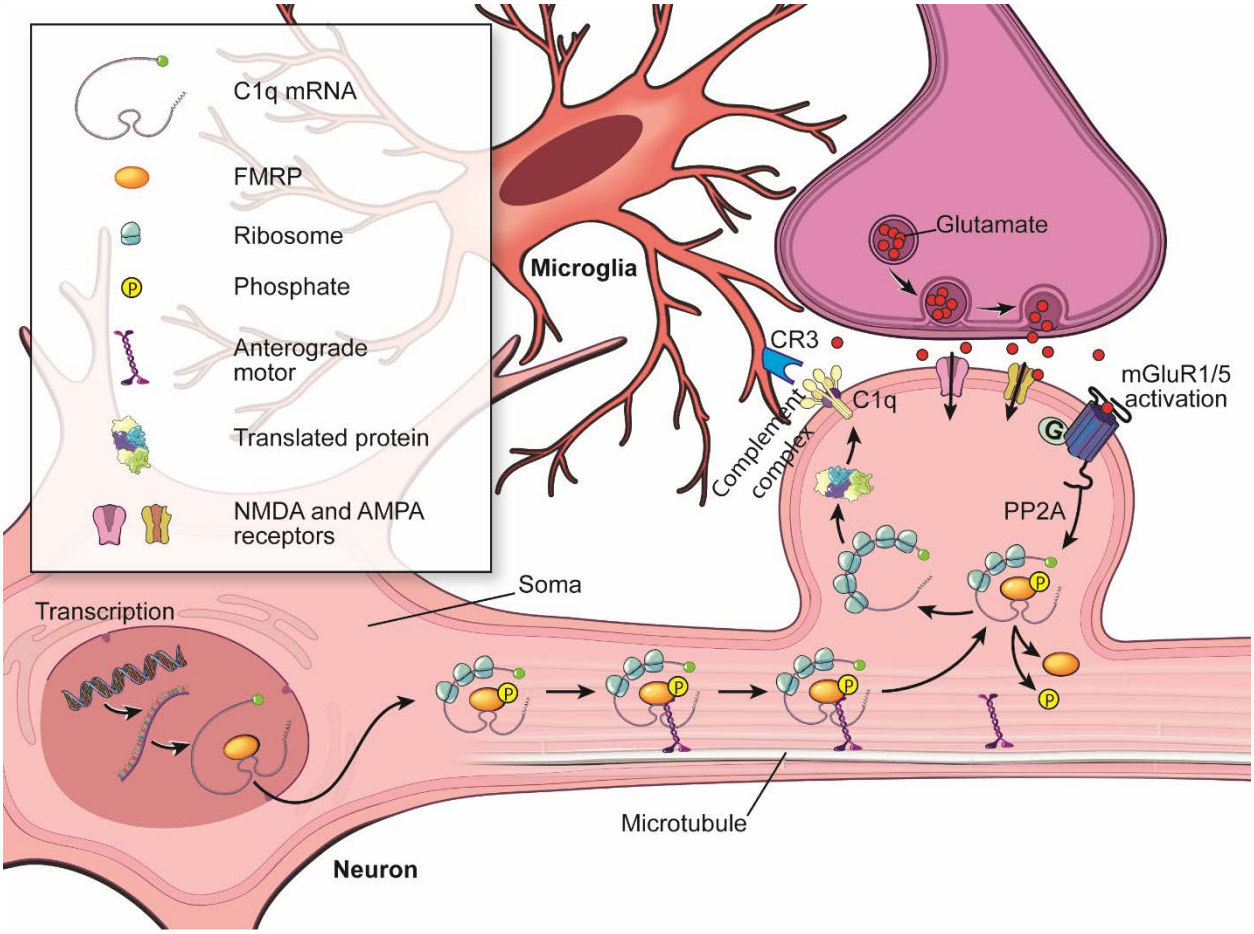

Figure 1. Hypothesis tested. Abnormal accumulation of amyloid fibrils induces substantial neuroinflammation (e.g., microglial activation) and the upregulation of mGluR1 signaling in the hippocampal CA1. Activation of mGluR1 signaling induces remarkable PP2A activity, which triggers the dephosphorylation of FMRP in the glutamatergic synapses. This adaptation of translational machinery, in turn, facilitates the transport and local translation of synaptic C1q mRNA in the glutamatergic synapses. The increased expression of C1q in glutamatergic synapses initiates the complement response leading to CR3 opsonization in the activated microglia, which eventually triggers the microglial phagocytosis of hippocampal glutamatergic synapses, thus contributing to the synaptic dysfunction and memory deficiency induced by amyloid fibrils.

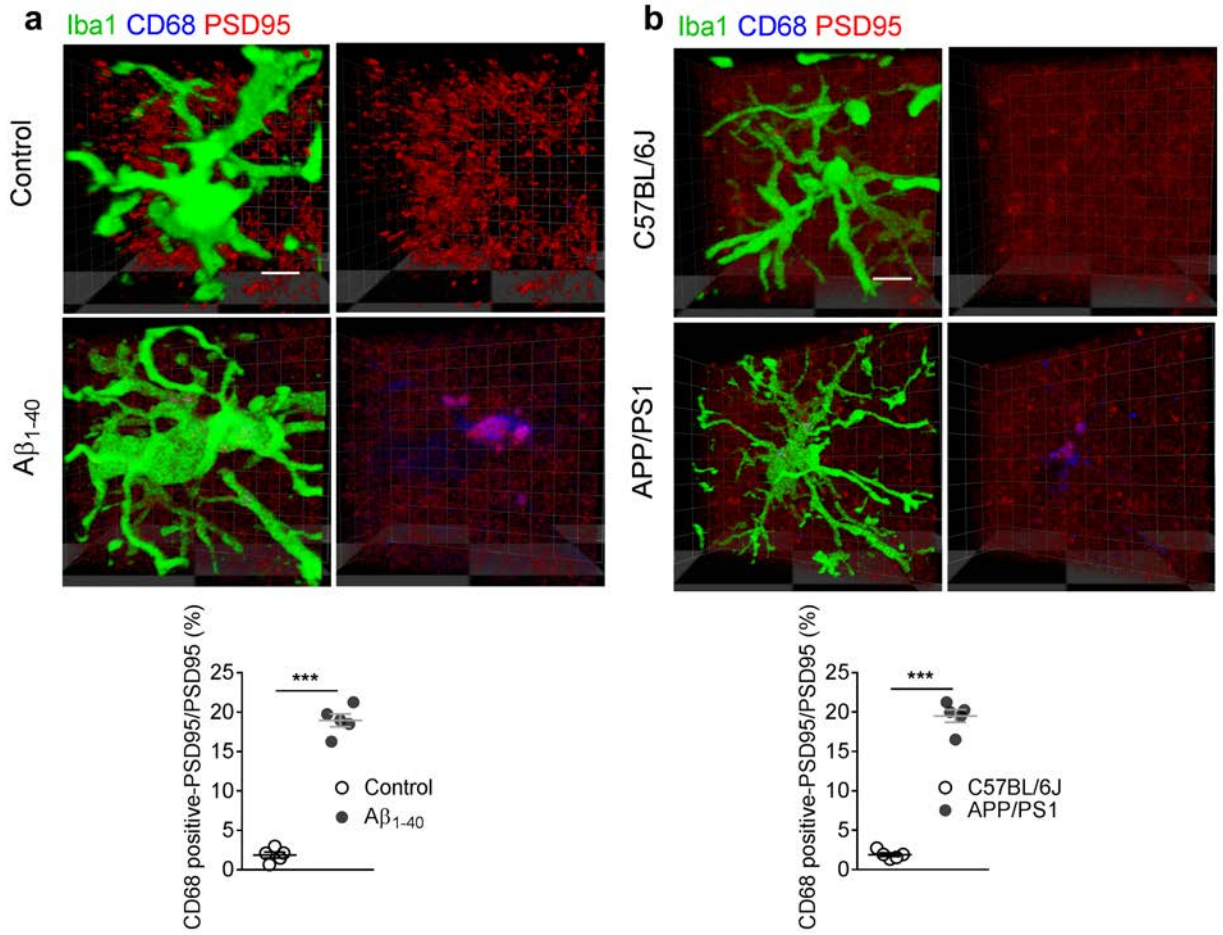

Figure 2. Increased microglial phagocytosis of glutamatergic synapses in rodent AD model. Increased internalization of postsynaptic marker PSD95 was observed in the lysosomes (CD68) within the microglia (Iba1) in the rats injected with $A\beta_{1-40}$ fibrils (***a***, n = 5 rats in each group, t = 18.9, DF = 8, two-tailed P <0.0001, scale bar = 10 μm). A micrograph was presented at the right to show the same microglia in which only the lysosomes (blue) and PSD95 (red) were visualized. Similar increases in co-localization of PSD95 with lysosome marker CD68 within the microglia were observed in the hippocampal CA1 of the Tg-APPsw/PSEN1DE9 (APP/PSI) mice (***b***, n = 5 mice in each group, t = 21.6, DF = 8, two-tailed P <0.0001, scale bar = 10 μm). Data represent mean ± s.e.m. ***P<0.001. Each dot represents the mean value of 4 brain slices of one animal.

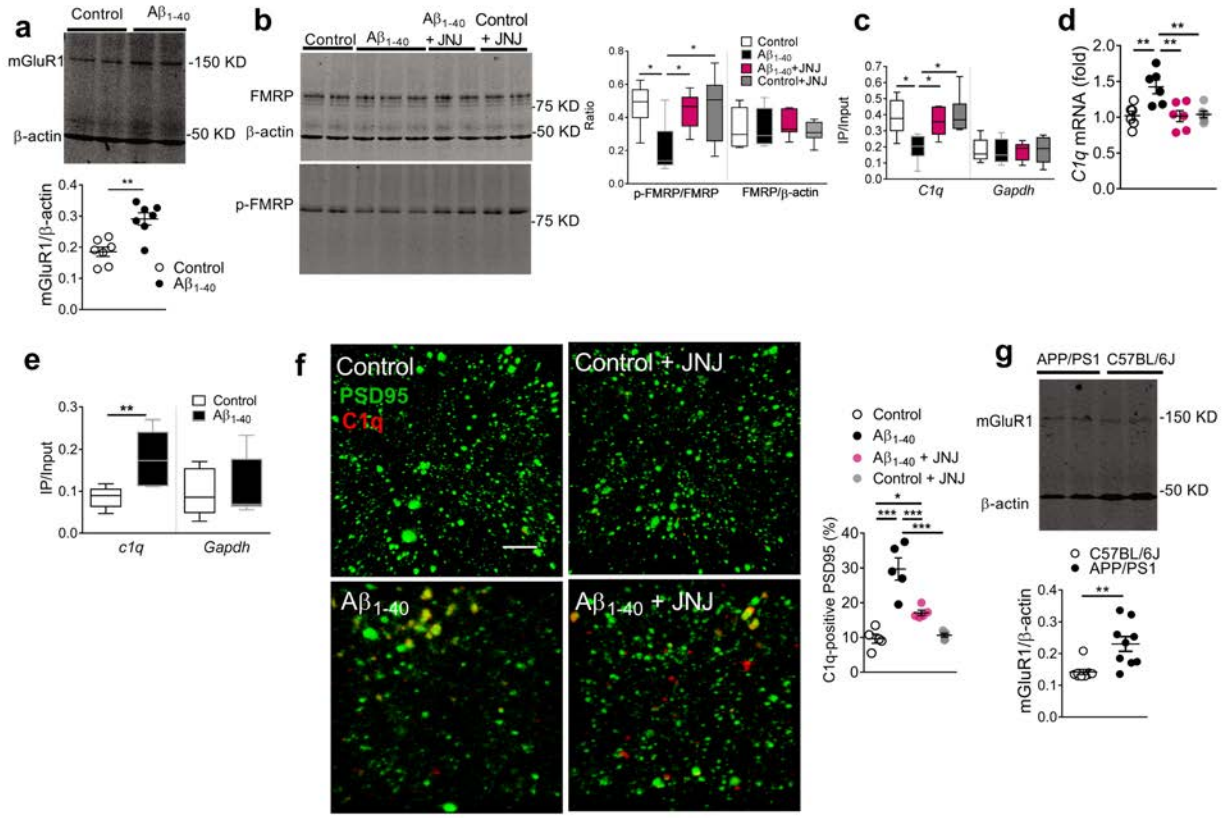

Figure 3. Inhibition of metabotropic glutamate receptor 1 (mGluR1) signaling attenuated the C1q upregulation induced by amyloid fibrils. Significantly increased expression of mGluR1 was observed in the hippocampal CA1 in the rats injected with amyloid fibrils (**a**, n = 7 rats in each group, t = 4.3, DF = 12, two-tailed P = 0.001). Amyloid fibrils decreased the phosphorylation of fragile X mental retardation protein (FMRP) in the hippocampal CA1, which was recovered by the mGluR1 inhibitor JNJ16259685 (**b**, n = 6,7,7,7 rats, $F_{3,23}$ = 4.3, P = 0.015); (**c**) RNA-IP study revealed a significantly decreased amount of C1q mRNA pulled-down by p-FMRP antibody in the hippocampal CA1 in the modeled rats, which was recovered by JNJ16259685 (**c**, n = 6 rats in each group, $F_{3,20}$ = 4.97, P = 0.009). Significantly increased *C1q* mRNA was detected in the hippocampal synaptosomal preparation in the modeled rats, which was attenuated by JNJ16259685 (**d**, n = 6 rats in each group, $F_{3,20}$ = 7.46, P = 0.002). Increased C1q mRNA was pulled by e-IF4E antibody in hippocampal CA1 lysates of the rats injected with amyloid fibrils (**e**, n = 6 rats per group, t = 3.3, DF = 10, two-tailed P = 0.009). For box-and-whiskers plots, the box extends from the 25th to 75th percentiles, a line within the box marks the median. Whiskers (error bars) above and below the box represent the minimum and maximum values. Microinjection of JNJ16259685 significantly decreased C1q immunosignals co-localized with the PSD95 in the hippocampal CA1 in the amyloid-injected rats (**f**, n = 5 rats in each group, $F_{3,16}$ = 26.5, P <0.0001, scale bar = 10 μm). Each dot represents the mean value of 4 brain slices of one rat. Significantly increased expression of mGluR1 was observed in the hippocampal CA1 in the Tg-APPsw/PSEN1DE9 (APP/PSI) mice (**g**, n = 9 mice in each group, t = 3.6, DF = 16, two-tailed P = 0.003). Data represent mean ± s.e.m. *P<0.05, **P<0.01, ***P<0.001.

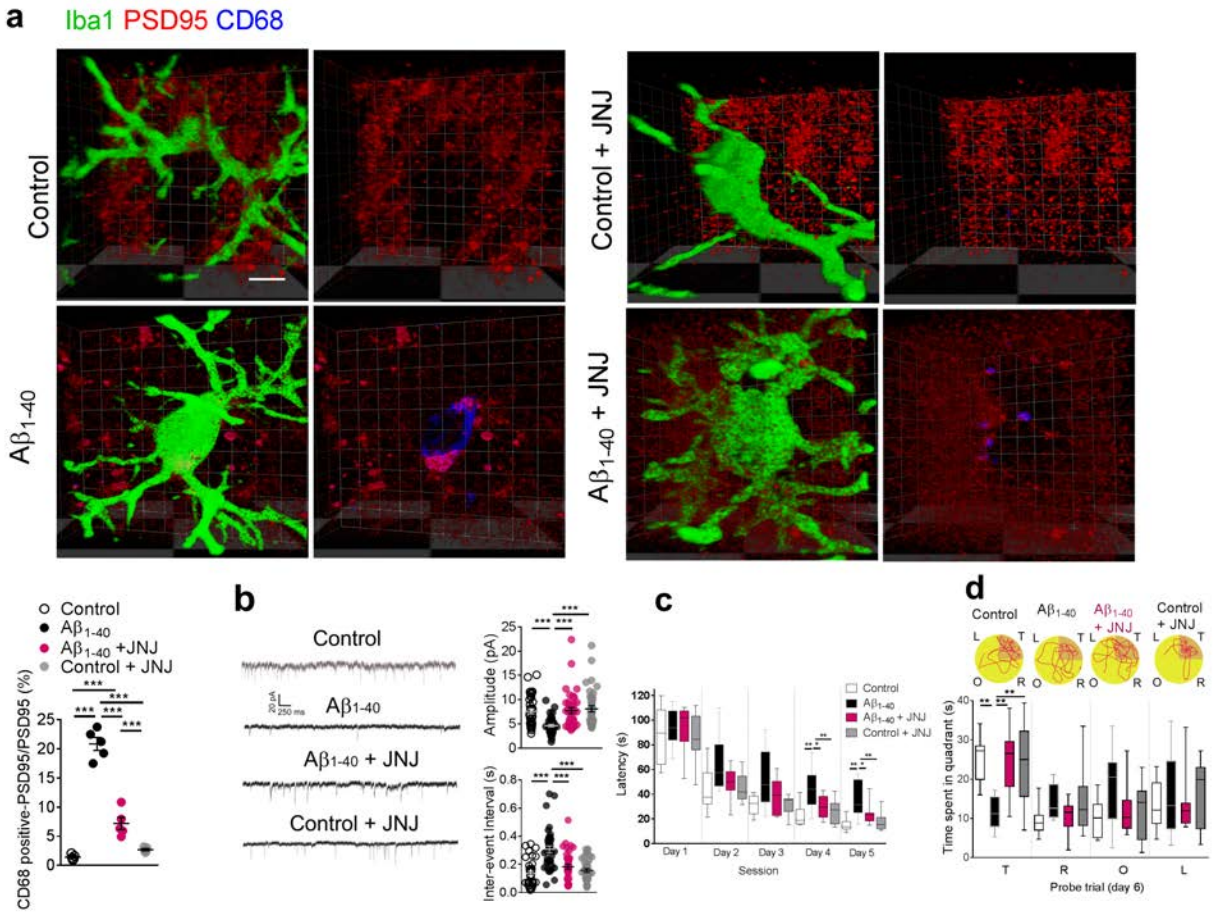

Figure 4. Inhibition of mGluR1 signaling attenuated the microglia phagocytosis of synapses induced by amyloid fibrils. JNJ16259685 significantly decreased the co-localization of PSD95 with lysosome marker CD68 in microglia (Iba1) in the rats injected with amyloid fibrils (**a**, n = 5 rats in each group, $F_{3,16} = 301.8$, $P < 0.0001$, scale bar = 10 μm). Right micrographs were presented to show the same microglia in which only the lysosomes (blue) and PSD95 (red) were visualized. Microinjection of JNJ16259685 significantly recovered the amplitude (**b**, n = 38 neurons in each group, Kruskal-Wallis Statistic KW = 33.6, P<0.0001) and inter-event interval of mEPSCs (**b**, n = 38 neurons in each group, Kruskal-Wallis Statistic KW = 37.9, P<0.0001) in the hippocampal CA1 neurons in the rats injected with amyloid fibrils. Microinjection of JNJ16259685 also shortened the escape latency (**c,** n = 10 rats in each group, effect of group [$F_{3,36} = 13.3$, P<0.0001], effect of time [$F_{4,36} = 135.5$, P<0.0001], interaction between group and time [P = 0.47]) and increased the time spent in the target quadrant (**d,** n = 10 rats in each group, $F_{4,36} = 6.57$, P = 0.0012) in the amyloid-injected rats. (**d**) Representative path tracings in each quadrant during the probe trial on day 6 (T, target quadrant; R, right quadrant; O, opposite quadrant; L, left quadrant). Data represent mean ± s.e.m. For box-and-whiskers plots, the box extends from the 25th to 75th percentiles, a line within the box marks the median. Whiskers (error bars) above and below the box represent the minimum and maximum values. *P<0.05, **P<0.01, ***P<0.001.

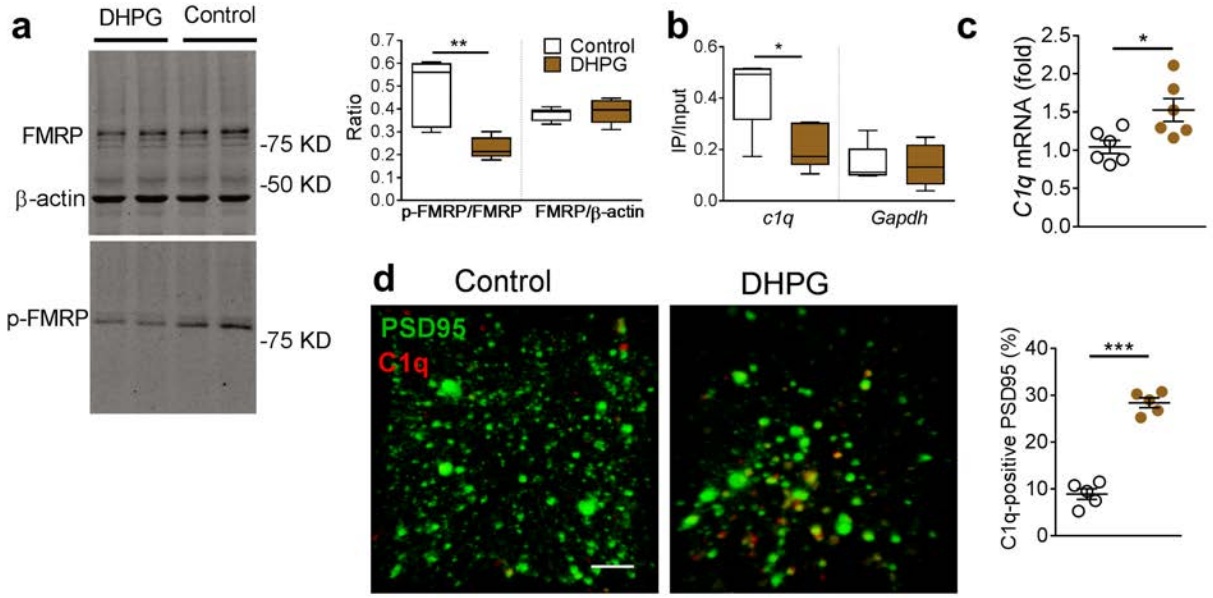

Figure 5. Activation of mGluR1 signaling by specific mGluR agonist dihydroxyphenylglycine (DHPG) upregulated hippocampal C1q expression. Microinjection of DHPG into the hippocampal CA1 in naïve rats induced dephosphorylation of FMRP (**a**, n = 6 rats in each group, Mann-Whitney U-statistic = 35.00, two-tailed P = 0.007), decreased the binding between phosphorylated FMRP (p-FMRP) and *C1q* mRNA (**b**, n = 6 rats in each group, Mann-Whitney U-statistic = 33.00, two-tailed P = 0.015), and increased *C1q* mRNA in the hippocampal CA1 synaptosome (**c**, n = 6 rats in each group, t = 2.8, DF = 10, two-tailed P = 0.018). DHPG also increased the C1q immunosignal co-localized with PSD95 in the hippocampal CA1 in the naïve rats (**d**, n = 5 rats in each group, t = 12.6, DF = 8, two-tailed P <0.0001, scale bar = 10 μm). Each dot represents the mean value of 4 brain slices of one rat. Data represent mean ± s.e.m. For box-and-whiskers plots, the box extends from the 25th to 75th percentiles, a line within the box marks the median. Whiskers (error bars) above and below the box represent the minimum and maximum values *P<0.05, **P<0.01, ***P<0.001.

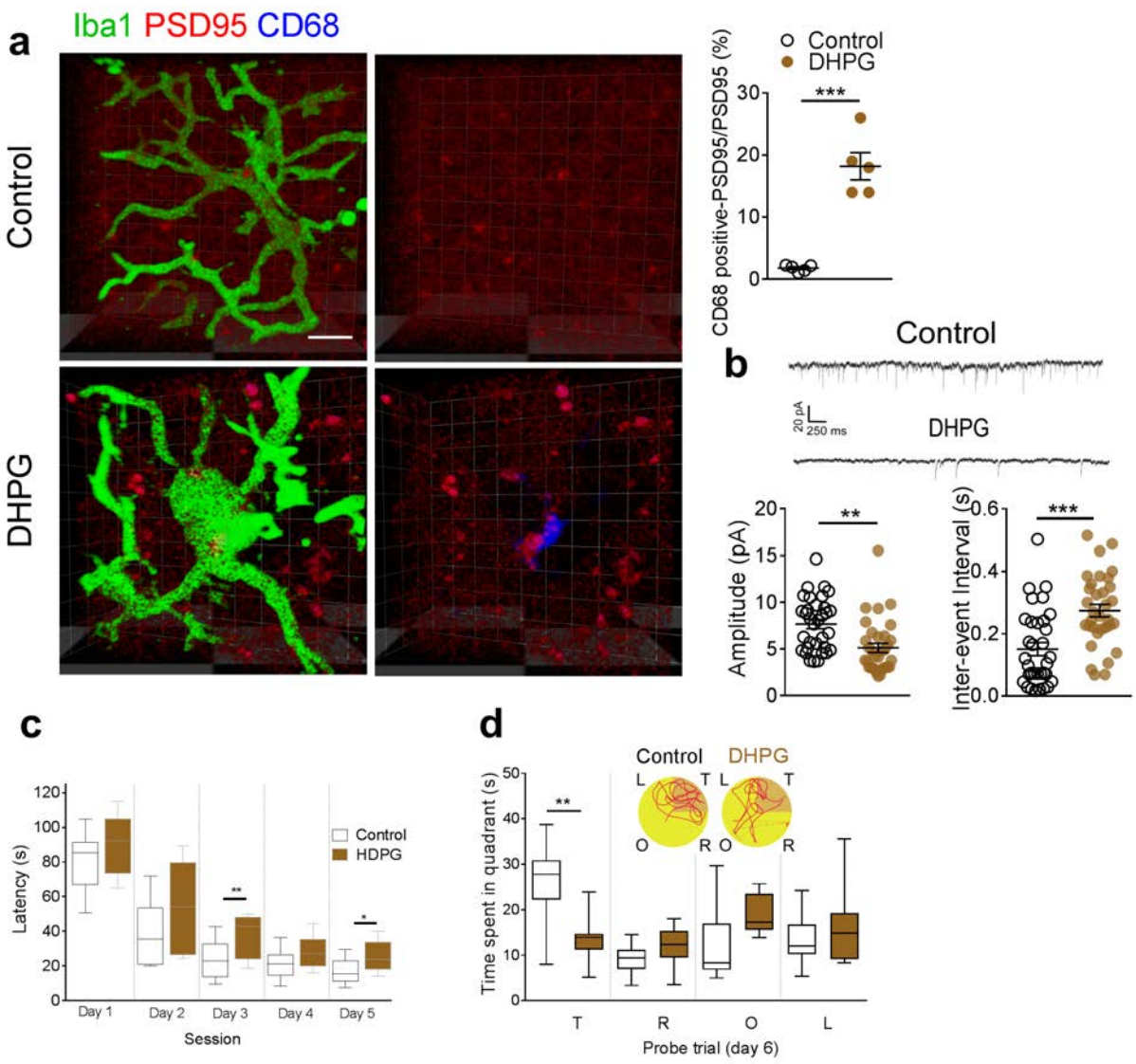

Figure 6. Activation of mGluR1 signaling by DHPG induced the microglial phagocytosis of glutamatergic synapses. DHPG increased the co-localization of PSD95 with the lysosome marker CD68 in microglia in the hippocampal CA1of naïve rats (**a**, n = 5 rats in each group, t = 7.4, DF = 8, two-tailed P <0.0001, scale bar = 10 μm). Right micrographs were presented to show the same microglia in which only the lysosomes (blue) and PSD95 (red) were visualized. Each dot represents the mean value of 4 brain slices of one rat. DHPG also decreased the amplitude (**b**, n = 33 neurons in each group, t = 3.7, DF = 64, two-tailed P = 0.0005) and increased inter-event interval (**b**, n = 33 neurons in each group, t = 4.2, DF = 64, two-tailed P <0.0001) of mEPSCs in hippocampal CA1 neurons, and increased escape latency (**c,** n = 10 rats in each group, effect of group [$F_{1,18}$ = 8.2, P = 0.01], effect of time [$F_{4,18}$ = 82.8, P<0.0001], interaction between group and time [P = 0.52]), and decreased the time in the target quadrant (**d**, n = 10 rats in each group, $F_{1,18}$ = 14.4, P = 0.001). (**d**) Representative path tracings in each quadrant during the probe trial on day 6 (T, target

quadrant; R, right quadrant; O, opposite quadrant; L, left quadrant). Data represent mean ± s.e.m. For box-and-whiskers plots, the box extends from the 25th to 75th percentiles, a line within the box marks the median. Whiskers (error bars) above and below the box represent the minimum and maximum values. *P<0.05, **P<0.01, ***P<0.001.

Amyloid Fibrils Induce Dysfunction of Hippocampal Glutamatergic Silent Synapses

Presenting Author: Mark Hocevar[1]

Co-Authors: Bihua Bie[1], Jiang Wu[1], Joseph Foss[1], Mohamed Naguib[1]

[1]Department of General Anesthesia, Anesthesiology Institute, Cleveland Clinic

Introduction: Extensive neuroinflammation in Alzheimer's disease (AD) causes neuronal and synaptic loss, resulting in cognitive impairments. The molecular mechanisms underlying amyloid-induced synaptic dysfunction remain an area of interest. Our hypothesis is that accumulation of amyloid species results in the impairment of cytoskeleton protein (e.g., cofilin) and PSD scaffolding protein (e.g., PSD95), which decreases the distribution of GluR1 anchoring at PSD and leads to the dysfunction of glutamatergic synapses in the hippocampal CA1 and impairment of synaptic plasticity and cognition.

Methods: Rats injected with amyloid fibrils into hippocampal CA1 were used in this study. The minimal stimulation-based silent synapse recordings were performed on the hippocampal CA1 neurons and the activation of silent synapses was induced by pairing low-frequency electric stimuli. Immunoblotting was used to study the expression of GluR1. Whole-cell recording and Morris water maze were used to evaluate the synaptic and cognitive function in the rodent models.

Results: First, we noted that Amyloid impairs the unsilencing of glutamatergic silent hippocampal synapses. The percentage of silent synapses in the hippocampal CA1 in rats injected with $A\beta_{1-40}$ was lower than that in rats injected with saline (**Fig. 1**). Next, we found the reduction of the immunosignal of GluR1 was observed in the hippocampal synaptosome in rats injected with $A\beta_{1-40}$ (**Fig. 2**). Then, Amyloid impaired cytoskeletal actin dynamics and postsynaptic scaffolding protein. Microinjection of $A\beta_{1-40}$ substantially decreased the expression level of phosphorylated cofilin (**Fig. 3**). In addition, microinjection of $A\beta_{1-40}$ markedly decreased the expression level of PSD95 in the hippocampal CA1 synaptosome (**Fig. 4**). Microinjection of amyloid fibrils reduced the hippocampal glutamatergic strength and high-frequency electric stimuli-induced long term potentiation in hippocampal CA1 neurons, and impaired the performance in Morris water maze test in rats (**Fig. 5**).

Conclusion: This study demonstrated a reduction of hippocampal silent synapses, which failed to be activated by pairing low-frequency stimuli in the rodent model of AD. These findings may, at least partially, result from the impairment of the actin cytoskeleton and PSD scaffold proteins in the central neurons.

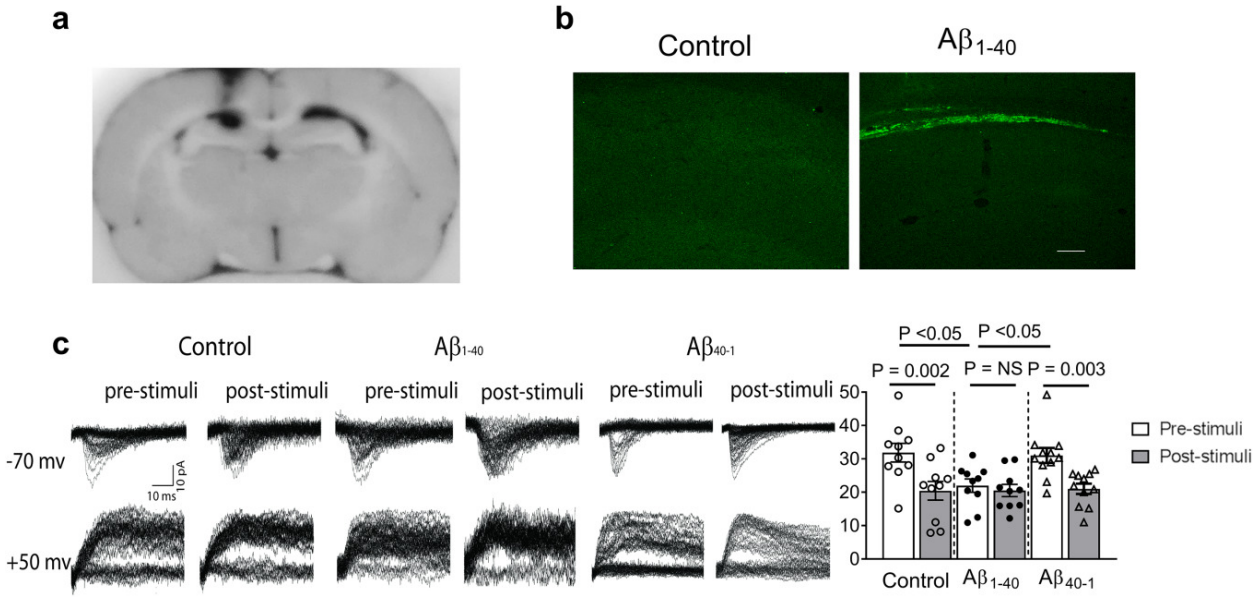

Fig. 1 Microinjection of $A\beta_{1-40}$ fibrils induced dysfunction of hippocampal silent synapses. (**a**) An India ink-marked microinjection site in the hippocampal CA1 area demonstrated the preciseness of the injection site. (**b**) Immunostaining images showed the existence of $A\beta_{1-40}$ in the rats injected with $A\beta_{1-40}$ after the completion of behavioral testing, which was clearly absent in the control rats. (**c**) EPSCs in the silent synapse appeared at baseline at a holding potential of +50 mV but not at –70 mV. After pairing with low-frequency electric stimuli, EPSCs appeared at –70 mV. The percentage of silent synapses among all recorded synapses was calculated as $1-Ln(F_{-70})/Ln(F_{+50})$, in which F_{-70} is the failure rate at -70 mV and F_{+50} is the failure rate at +50 mV. The percentage of silent synapse (within groups) was compared using paired t-test in the control group ($t = 4.515$, $DF = 9$, two-tailed $P = 0.002$), $A\beta_{1-40}$ group ($t = 0.72$, $DF = 9$, $P = 0.49$), and $A\beta_{40-1}$ group ($t = 3.98$, $DF = 10$, $P = 0.003$). Pre-stimuli were compared among the groups using one-way ANOVA ($F = 5.25$, $DF = 30$, two-tailed $P = 0.012$). Data represent mean ± s.e.m.

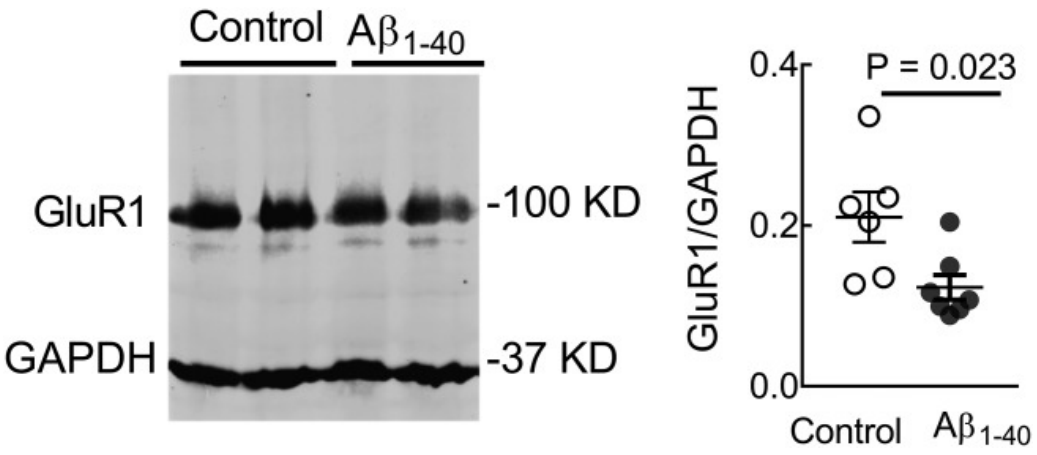

Fig. 2 Significantly decreased expression of AMPA receptor subunit GluR1 in the hippocampal CA1 synaptosomal preparation, which indicated a reduced distribution of GluR1 in glutamatergic synapses, in rats injected with $A\beta_{1\text{-}40}$ ($t = 2.63$, $DF = 11$, two-tailed $P = 0.023$). Data represent mean ± s.e.m.

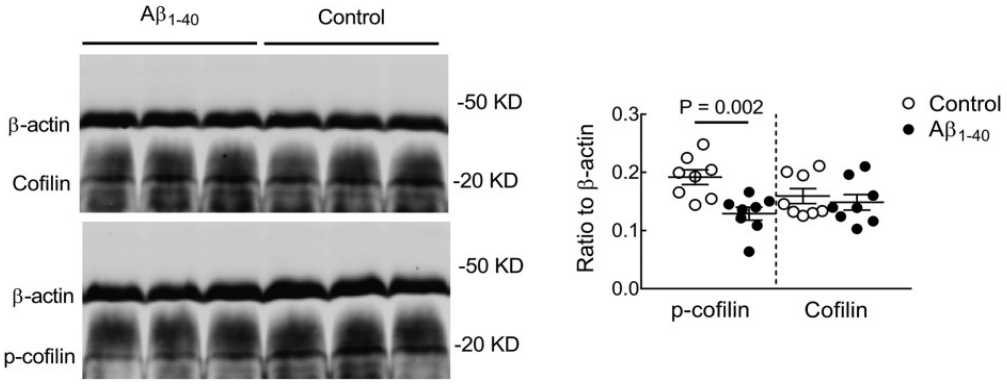

Fig. 3 Microinjection of $A\beta_{1\text{-}40}$ significantly decreased the expression of phosphorylated cofilin ($t = 3.74$, $DF = 14$, two-tailed $P = 0.002$), but not that of total cofilin ($t = 0.58$, $DF = 14$, two-tailed $P = 0.6$), in the hippocampal CA1 in rats injected with $A\beta_{1\text{-}40}$. These results indicated a potential dysfunction of actin cytoskeleton in hippocampal CA1 in the modeled rodents. Data represent mean ± s.e.m.

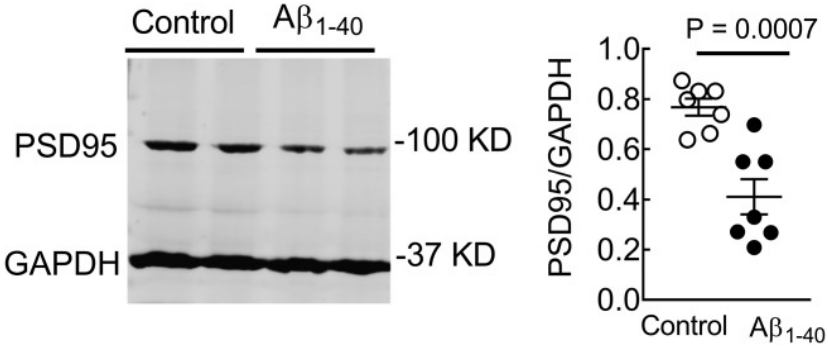

Fig. 4 Significantly decreased the expression of scaffolding protein PSD95 in hippocampal CA1 synaptosomal preparation in rats injected with amyloid fibrils (t = 4.56, DF = 12, two-tailed P = 0.0007). This potentially contributed to the dysfunction of hippocampal silent synapses in the rat injected with A□$_{1-40}$. Data represent mean ± s.e.m.

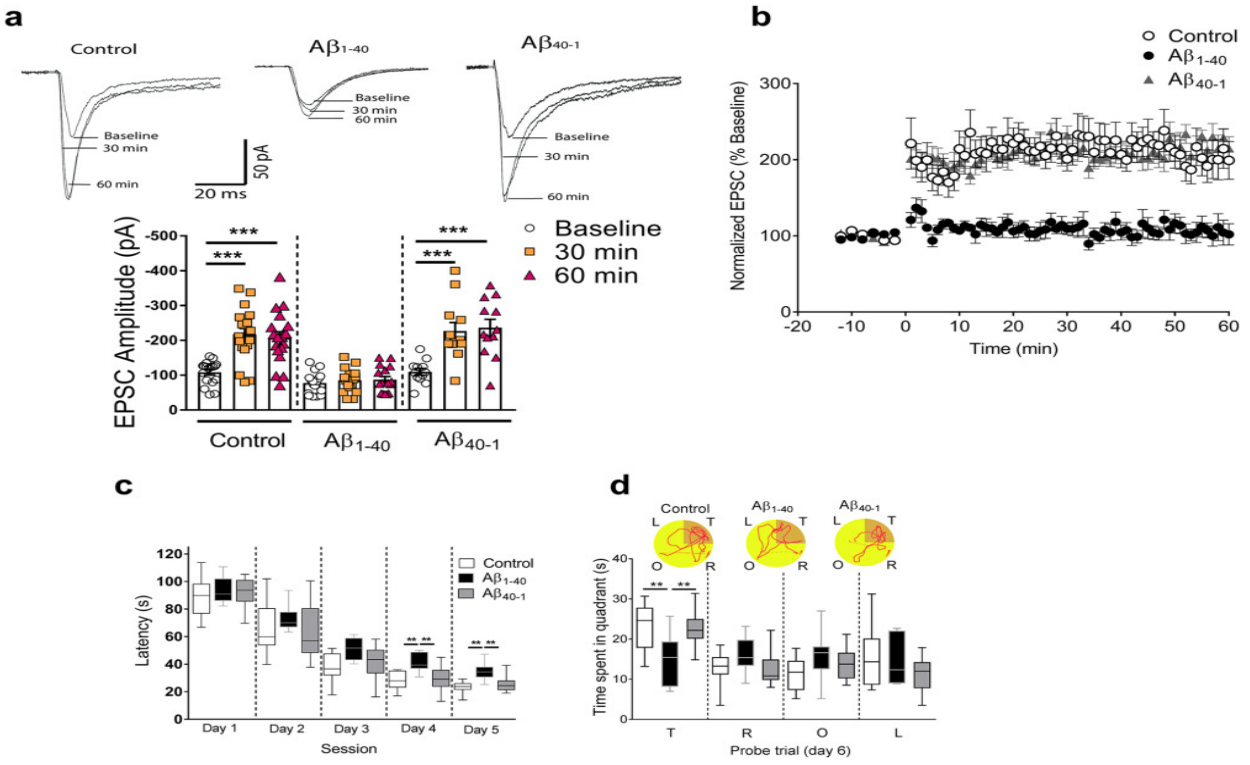

Fig. 5 Hippocampal injection of A$\beta_{1–40}$ fibrils impaired memory and glutamatergic synaptic plasticity. (a-b) Significantly impaired long-term potentiation (LTP) in the hippocampal CA1 neurons induced by microinjection of Aβ_{1-40}. LTP was induced by electric stimuli on the Schaffer collateral–commissural fibers at 100 Hz for 1 second. (a) The representative traces of EPSCs were presented to show the evoked EPSCs at baseline, 30, and 60 minutes after electric induction. Data were analyzed with repeated measures ANOVA. (a) Control group (n = 18, $F_{2,17}$ = 42.8, P<0.0001), A$\beta_{1–40}$ group (n = 16, $F_{2,15}$ = 0.53, P = 0.6), and Aβ_{40-1} group (n = 12, $F_{2,11}$ = 40.2, P<0.0001). (b) Time course of the amplitude of EPSCs in all three groups (b, n = 18, 16 and 12 neurons in each group, $F_{2,43}$ = 18.7, P<0.0001). (c-d) Significantly extended escape latency (c**,** n = 10 rats in each group, effect of group [$F_{2,27}$ = 7.71, P<0.002], effect of time [$F_{4,27}$ = 200.9, P<0.0001], interaction between group and time [P= 0.47]) and less time spent in the target quadrant (d, n = 10 rats in each group, $F_{2,27}$ = 6.67, P = 0.004) in rats microinjected with A$\beta_{1–40}$ fibrils but not Aβ40-1 fibrils nor artificial CSF (control). Representative path tracings in each quadrant during the probe trial on day 6 (b, T, target quadrant; R, right quadrant; O, opposite quadrant; L, left quadrant). **, P<0.01. Data represent mean ± s.e.m. For box-and-whiskers plots, the box extends from the 25th to 75th percentiles, a line within the box marks the median. Whiskers (error bars) above and below the box represent the minimum and maximum values.

The Nociception Index (qNOX) Correlated with Hypothermia During Cardiopulmonary Bypass

Presenting Author: Pablo Martinez-Vazquez[1]

Co-Authors: Xiaohua Wang [2,3,4], Jinfeng Zhang [2,3,4], Wenwei Qi[5], Chaoran Nie [2,3,4], Bei Liu [2,3,4], Zhaolong Tian [2,3,4], Guoguang Zhao [2,3,4], Tianlong Wang [2,3,4]

[1] German Primate Center (DPZ), Leibniz Institute for Primate Research, Göttingen. Germany

[2] Institute of Geriatrics, Beijing, China

[3] National Clinical Research Center for Geriatric Disorders, Beijing, China

[4] Department of Anesthesiology, Xuanwu Hospital, Capital Medical University, Beijing 100053, China

[5] Department of Medical Informatics, Academic Medical Centre, University of Amsterdam, Meibergdreef 15, 1105 AZ Amsterdam, the Netherlands.

Introduction: The depth of anesthesia is commonly assessed by the patient's clinical signs, based on surrogate parameters, which have low specificity in detecting nociceptive stimuli; this can result in under dosage or over-dosage of anesthetic agents [1]. The qNOX is a derived EEG index implemented in the Conox monitor (Fresenius Kabi, Bad Homburg, Germany) which measures the probability of the patient to respond to external noxious stimuli, providing an objective measurement of the patient's analgesia state [2].

The non-appreciable gain in blood pressure (BP), heart rate (HR) or even body movements during surgery, in particular during cardiopulmonary bypass (CPB) and hypothermia, suggest the difficult determination of nociception. The aim of this study is to evaluate the effectiveness of the qNOX index under induced hypothermia during the CPB.

Methods: The qNOX was recorded during general anesthesia for 39 patients with coronary atherosclerosis cardiopathy who were scheduled for elective on-pump coronary artery bypass graft (CABG) surgery under hypothermia and cardiopulmonary bypass (CPB) at the Xuanwu Hospital, after approval of the local IRB. Two depth of sedation EEG derived indexes, qCON and Bispectral Index (BIS) [3] were also recorded. The patients were ranging in age from 35 to 80 years, with an American Society of Anesthesiologists (ASA) Physical Status score of 1 to 3 and a body mass index (BMI) ranging from 18.5 to 35 kg/m2. Anesthesia was administered using etomidate 0.2 mg/kg; sulfentanyl 1 μg/kg; rocuronium 1 mg/kg. CPB was established when the nasopharyngeal temperature reached 31–32°C; α-stat acid-base management strategy during nasopharyngeal temperature of ≥30°C. The changes and correlation between qNOX and temperature were compared in different time points at basic state, during and after CPB.

Results: The qNOX values during CPB at 5, 10, 15 and 20 minutes after CPB was established were significantly lower than the values at Enter OR ($p < 0.01$), incision, ($p < 0.01$), induction ($p < 0.01$), at 5, 10, 15 min pre-CPB ($p < 0.01$) and at 5, 10 and 15 min Post-CPB time points ($p < 0.01$) (**Fig. 1A**). The temperature level also was significantly reduced compared to the previous time points at Enter OR ($p < 0.01$), incision, ($p < 0.01$), induction ($p < 0.01$), pre-CPB ($p < 0.01$) and Post-CPB (**Fig. 1B**). After CPB, both temperature and qNOX returned to baseline pre-CPB levels. From induction of anesthesia to CPB establishment, there was a little fluctuation of qCON (**Fig. 1C**), but BIS did not decrease much during this period (**Fig. 1D**). The correlations between the three EEG indexes (qNOX, qCON and BIS) and the nasopharyngeal temperature were estimated by linear regression (**Fig. 2**). The qNOX showed a strong positive correlation with temperature (R^2=0.71; *P*<0.01. **Fig. 2A**) with a low-to-moderate correlation between qCON and temperature (R^2=0.30; *P*<0.01. **Fig. 2B**). BIS exhibited a very weak correlation with the temperature during the whole operation (R^2=0.095; *P*<0.01**. Fig. 2C**).

Conclusion: The nociception index, qNOX, revealed a high positive correlation with the temperature, which was higher than the correlations of the temperature with the sedation indexes, qCON and BIS. The results suggest that hypothermia may potentiate the depth of analgesia and the nociception index qNOX, in combination with qCON, can effectively reflect the analgesia and hypnosis levels during the CPB surgery period.

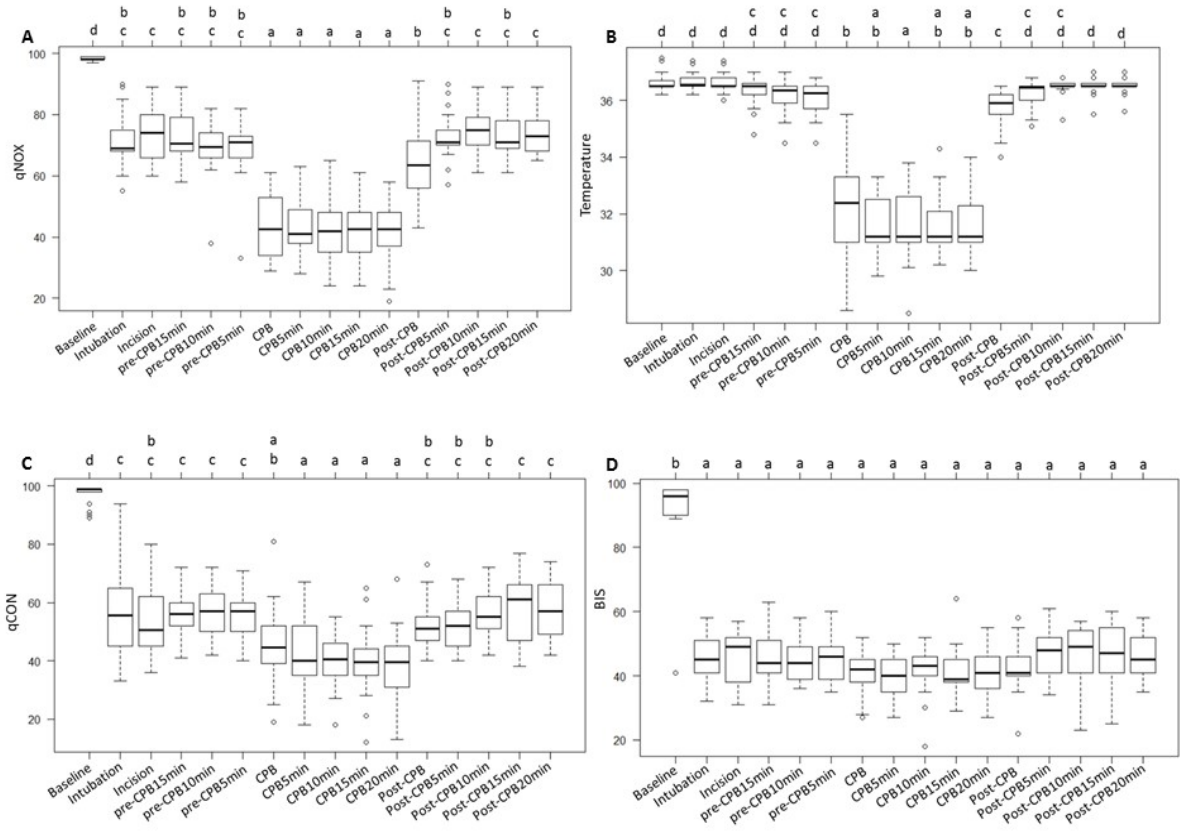

Figure 1. *Percentile boxplots of qNOX (A), qCON (B), Temperature (C) and BIS (D) during CABG surgery. Note: The letters (a, b, c, and d) on top of the boxplots*

represent the significant differences at distinct timepoints. There are no significant differences among timepoints with the same letters, while timepoints with different letters indicate significant differences.

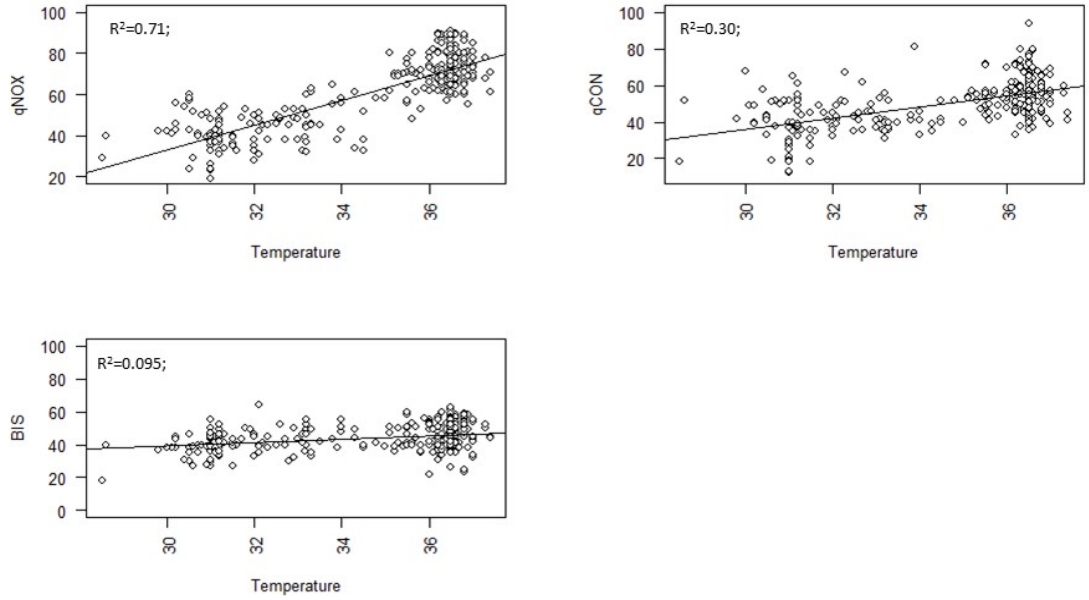

Figure 2. *Scatter plots for the correlation between qNOX and Temperature (A), qCON and Temperature (B), and BIS and Temperature (C).*

References

1. Gambús PL, Jensen EW, Jospin M, Borrat X, Pallí GMn, Fernández-Candil J et al. Modeling the effect of propofol and remifentanil combinations for sedation-analgesia in endoscopic procedures using an adaptive neuro fuzzy inference system (anfis). *Anesthesia & Analgesia* 2011;112:331-339.

2. Jensen EW, Gambus PL, Valencia JF, Jospin M, Borrat X, Struys M et al. Validation of the qnox pain/nociception index for monitoring loss of response to tetanic stimulation during general anaesthesia. *Anesthesiology* 2013;119.

3. Avidan MS, Mashour GA. Prevention of intraoperative awareness with explicit recall making sense of the evidence. *Anesthesiology* 2013;118:449-456.

Proposing a More Optimal Methadone Induction Strategy

Presenting Author: Elie Sarraf[1]
Co-Authors: Donald M. Mathews[1]

[1]University of Vermont College of Medicine, Burlington, Vermont

Introduction: Methadone is a long acting opioid with NMDA receptor antagonist properties which has been commonly used for both chronic pain and as a drug detoxification for opioid abuse. Methadone induction is a clinical challenge due to its long and variable half-life [1-4] thus requiring many days to achieve steady state. While only 1% of opioid users take methadone, it accounts for over 20% of opioid-related deaths [5]. While the present recommendations are to titrate slowly, we argue that if a given patient's methadone pharmacokinetics can be estimated, one can more rapidly achieve steady state with an optimal induction dosing strategy.

Methods: The appendix outline the induction strategy and involves: 1) estimation of the terminal elimination rate constant, β after a test dose and blood sampling and 2) creating an induction dose by using, in part, the accumulation index [6].

Using Matlab (R2017b), we compared the performance of the induction strategy to standard induction. Patient were simulated with T ½ α between 1.5 and 4.2 hours and T ½ β between 8.5 and 65 hours. The value were randomly selected using a truncated Normal distribution. A test dose was simulated and sampled at the 24 hour and 48 hour interval. The samples were given measurement errors with coefficient of variation of 3% [7]. β was estimated and limited to achieve a T ½ β between 8.5 and 65 hours.

Four different induction sequence were simulated on the same patient at a time: daily dosing, q8h dosing, daily dosing with optimal induction, q8h dosing with optimal induction. The total simulation time was 30 days, sampled every 15 minutes.

The following parameters were measured: time to converge to within 10% of the steady state trough (settling time), maximum blood concentration and time at which it occurred. Analysis was performed with Wilcoxon signed-rank test.

Results: 100,000 patients were simulated. Median settling time for the optimal daily and q8h dosing were both 16 hours, which contrasts with the settling time for the standard dosing regimen: 144 hours for daily dosing and 128 hours for q8h ($p < 1E\text{-}16$). Settling time is achieved in 48 hours for 91% and 93.9% of daily and q8h dosing respectively. Figure 1 shows the distribution of settling times for all four regimens. Incidence of overshoot greater than 20% is 0.69% for the daily dosing regimen and 1.5% for q8h dosing. These would occur between the 28th and 32nd hour and 11th and 28th hour respectively

Conclusion: The optimal induction strategy for methadone provides a rapid induction with a predictable peak effect. This can potentially decrease the harm caused by either delayed steady state or patient self-medication leading to overdose. Its performance in clinical practice has yet to be determined.

References

1. Nilsson MI et al. Acta Anaesthesiol Scand Suppl. 1982:74: 66-69
2. Meresaar U et al. Eur J Clin Pharmacol. 1981: 20(6): 473-478
3. Wolff K et al. Eur J Clin Pharmacol. 1993: 44(2): 189-194
4. de Vos JW et al. Eur J Clin Pharmacol. 1995: 48(5):361-6.
5. Faul M et al. MMWR Morb Mortal Wkly Rep 2017: 66:320–323
6. Multiple Dose Regimens in Rowland M et al, Clinical Pharmacokinetics and Pharmacodynamics Concepts and Applications. 2010: 4th Ed. LWW
7. Foster DJ et al. Ther Drug Monit. 2006 Aug: 28(4):559-67.

Appendix: Optimal Methadone induction strategy
There are two phases to the induction:

1) After giving a small test dose the patient blood level of R-methadone is measured over the next few days to estimate the terminal elimination rate constant, β (in 1/hour) . At a minimum two blood levels should be measured with enough time between them to have an appreciable change in blood concentration. If two samples are taken, β can be estimated as follows:

$$\beta = \frac{\ln(C(t_1)) - \ln(C(t_2))}{t_2 - t_1}$$

With $C(t_1)$ being the blood concentration of the drug at time t_1. For β values at or beyond the margins of a typical population, additional blood samples may be required.

2) The Induction sequence makes use of the accumulation index [6] for periodic drug dosing with a period T (in hours):

$$R_{ac}(\beta, T) = \frac{1}{1 - e^{-\beta T}}$$

For 8 hour dosing (q8h), one multiplies the first dose of the drug by R_{ac} (β,8) and then proceeds with the desired maintenance dose. For daily dosing, while one can multiply the first dose by R_{ac}(β,24). Alternatively, to minimize overshoot from model mischaracterization, one can start the first 24 hours by providing three doses every 8 hours as follows:

   a) The initial dose is the maintenance dose multiplied by $e^{-\beta(24-8)} * R_{ac}(\beta, 24)$
   b) The next two doses are multiplied by $e^{-\beta(24-8)} * R_{ac}(\beta, 24)/R_{ac}(\beta, 8)$
   c) All doses thereafter will be the desired maintenance dose

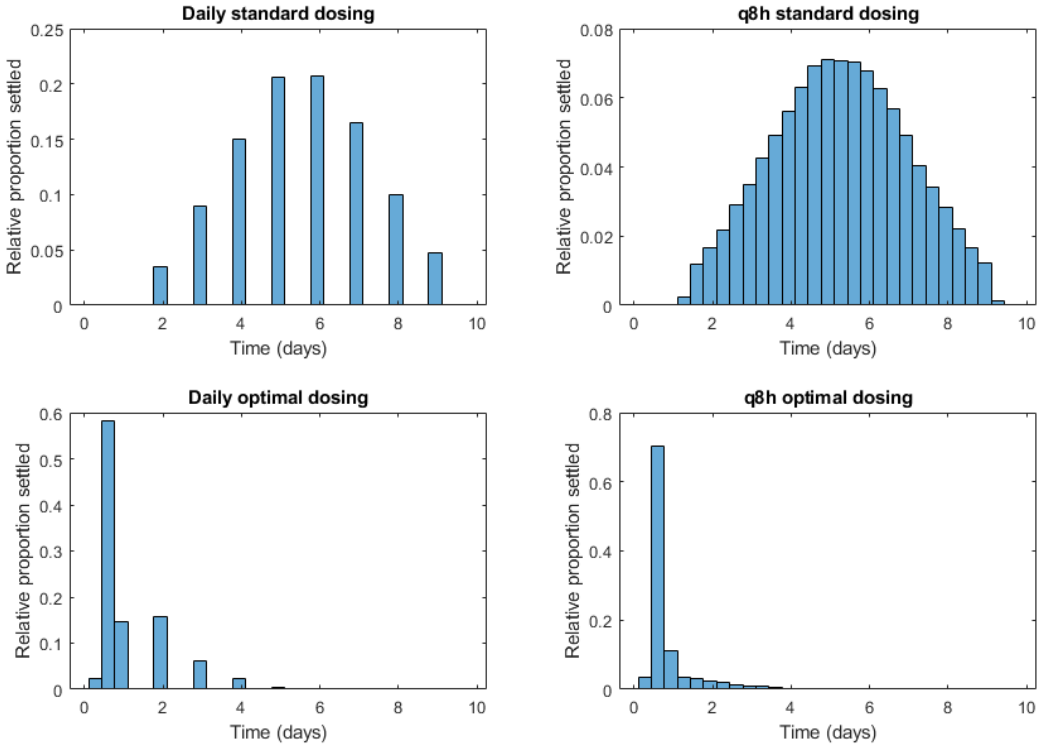

Figure 1: relative histogram of settling time for standard daily dosing, standard q8h dosing, daily dosing with optimal induction, q8h dosing with optimal induction

Minimal Sampling Strategy to Estimate the Terminal Elimination Rate Constant

Presenting Author: Elie Sarraf[1]
Co-Authors: Donald M. Mathews[1]

[1]University of Vermont College of Medicine, Burlington, Vermont

Introduction: Methadone is a long acting opioid with NMDA receptor antagonist properties which has been commonly used for both chronic pain and as a drug detoxification for opioid abuse. Methadone induction is a clinical challenge due to its long and variable half-life [1-4] thus requiring many days to achieve steady state. In a separate abstract we describe an optimal methadone induction strategy by identifying the terminal elimination rate constant (β) of the patient using a small initial dose followed by a dosing strategy using the accumulation index. We seek to determine the error of estimating β using a minimal sampling strategy that can be performed routinely on an outpatient basis and measure the impact of the error on this induction strategy.

Methods: Using Matlab (R2017b), we simulated the blood levels of 1,000,000 patients after a single test dose of methadone. The value of T½α and T½β were randomly generated using a uniform random distribution with values between 1.5 and 4.2 hours and 8.5 and 120 hours respectively. The blood levels were sampled after the test dose of methadone. 3%, 4%, 5% and 7% coefficient of variation error was added to the sampled values. β was calculated in one of two manners:

1) Using the two samples and direct computation:
$$\beta = \frac{\ln(C(t_1)) - \ln(C(t_2))}{t_2 - t_1}$$
With C(t) being the measured plasma concentration at time t.
This method was applied to measurements that were sampled at a) 24 and 48 hours, and b) 24 and 72 hours.
2) Three samples collected at 24, 48 and 120 hours were used to identify the parameters B and β in the equation $C_e(t) = Be^{-\beta t}$ such that it would minimize the following equation:
$$f(B,\beta) = \sum_i \left(\frac{C_e(t_i) - C(t_i)}{C_e(t_i)} \right)^2$$

Once the value of β was estimated, the optimal daily dosing strategy was applied to those simulated patients to determine the time for the methadone trough to be within 10% of the steady state trough (time to convergence). Also determined were the values of β that had a non-zero probability of having a 50% overshoot.

Results: Figure 1 shows the residual error plot between actual and the estimated values of β. Table 1 shows the mean and standard deviation of the residuals. The impact of the estimated β on the final time to convergence is shown in Figure 2. Table 2 shows the maximum T½β estimates that would ensure 0% probability of greater than 50% overshoot, while values above those listed in the table would have a progressively increasing risk of overshoot.

Discussion: As would be expected, one can improve the β estimates by increasing the number of samples collected, increasing the delay between samples and using a laboratory device that provides more precise measurements. Given that the vast majority of real patient T½β values of methadone are below 60 hours (beta = 0.011/hr) [1-4], one can effectively generate a minimal simple dosing strategy provided one has a well characterized laboratory device. This analysis will allow clinicians to have an appropriate margin of safety when dosing methadone through the optimal methadone induction strategy.

References

1. Nilsson MI et al. Acta Anaesthesiol Scand Suppl. 1982:74: 66-69
2. Meresaar U et al. Eur J Clin Pharmacol. 1981: 20(6): 473-478
3. Wolff K et al. Eur J Clin Pharmacol. 1993: 44(2): 189-194
4. de Vos JW et al. Eur J Clin Pharmacol. 1995: 48(5):361-6.

Figures and Tables

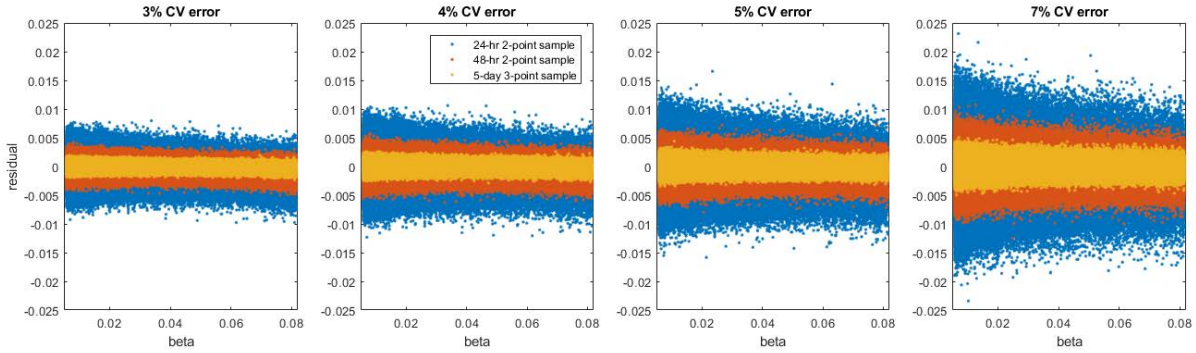

Figure 1: residual plot of β estimates

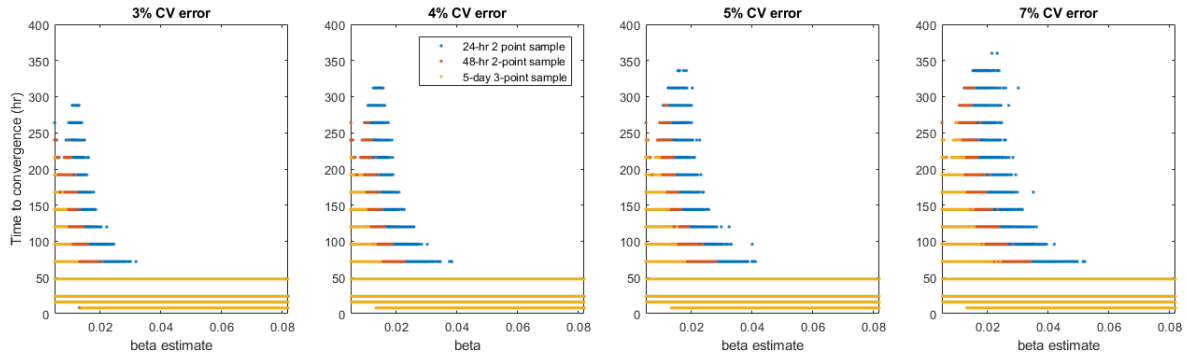

Figure 2: scatter of plot of time to convergence as a function of the estimated β

Beta residuals x 1000				
		Sampling method		
		24 hr	48 hr	3 points
%CV error	3%	0.34 +/- 1.82	0.17 +/- 0.91	0.06 +/- 0.43
	4%	0.34 +/- 2.40	0.17 +/- 1.20	0.06 +/- 0.57
	5%	0.35 +/- 2.99	0.18 +/- 1.49	0.05 +/- 0.72
	7%	0.34 +/- 4.18	0.18 +/- 2.09	0.04 +/- 1.00

Table 1: residual error of the β estimates. All values were multiplied by 1000

Critical estimated T1/2 β (hours)				
		Sampling method		
		24 hr	48 hr	3 points
%CV error	3%	56.66062	101.6738	
	4%	52.22409	82.94461	153.2405
	5%	36.35486	76.72882	143.378
	7%	31.3061	44.90001	105.2546

Table 2: Critical estimated T1/2 β values that would lead to 0% chance of 50% overshoot.

Monitoring Depth of Anaesthesia with the Conox

Presenting Author: Erik W Jensen[1]
Co-Authors: Isabel Serra[1], Umberto Melia[1], Pedro L Gambús[2]

[1]Quantium Medical SL, Mataró, Spain
[2] SPEC-M Lab of the Anesthesiology Dept., Hospital Clínic, Univ. Barcelona, Barcelona, Spain

Introduction: The electroencephalogram (EEG) has been studied to develop a reliable measure of the effects of the anesthetic agents in surgical procedures; a proper evaluation of the EEG during surgery is known to be a good predictor of the real physiological state of the patient [1]. The qCON is an index implemented in the Conox (Fresenius Kabi, Bad Homburg, Germany), which gives a prediction of the hypnotic level directly from the frontal EEG of patients under general anesthesia. The objective of this study is to validate the qCON index performance during surgical procedures by comparing it with the bispectral index (BIS) (Covidien, Boulder, CO, USA), and with clinical signs.

Methods: The EEG signals, qCON, BIS, anaesthetic agent concentrations and hemodynamic parameters were recorded simultaneously from a total of 1000 patients scheduled for ambulatory major surgeries in Hospital Clínic (Barcelona) undergoing general anesthesia with propofol and remifentanil, after approval of the local IRB. The target controlled infusion (TCI) system (Base Primea, Fresenius Vial, Brézins, France) administered the anaesthetic agents following the predictions of pharmacokinetic-pharmacodynamic models. Propofol (Ce prop) was infused following the Schnider model [2] and remifentanil (Ce remi), following the Minto model [3].
Clinical signs of loss of consciousness (LOC), such as loss of response to verbal command and loss of eyelash reflex were recorded during surgery. Prediction probability (Pk) has been computed for both qCON and BIS indices to compare two different anaesthetic states: the mean value during three minutes before LOC against the mean value three minutes after LOC. Acquired data with low signal quality index (SQI<50) were rejected. The relation between qCON and BIS indices was analyzed with Pk and Bland-Altman plot. Only the periods with Ce values in steady state were included in the analysis. The Pk and its standard error (SE) were computed taking the pool of data of qCON and BIS of all the recorded patients. The BIS was used as the reference: BIS values were divided in 4 levels (100-80; 80-60; 60-40; 40-0) and the histogram was equalized taking 45000 random points of each level.

Results: The obtained Pk between qCON and BIS indices of the 1000 registers is 0.8898 ± 0.0001. Figure 1 represents a boxplot of the qCON values against the BIS divided in 10 levels.

The distribution of the values of qCON and BIS of all the data pool is represented by the Bland- Altman analysis in figure 2. The mean values and standard deviation (SD) of the qCON and BIS indices three minutes before and after LOC are shown in the first and second column of table 1. The Pk's for qCON and BIS vs LOC are shown in the third column of table 1.

Conclusions: The qCON index shows a good agreement with the BIS index, as a predictor of the level of consciousness during general anesthesia. Clinical signs evaluated during surgery corroborate that qCON is a validated index for predicting the probability of the patient of being awake.

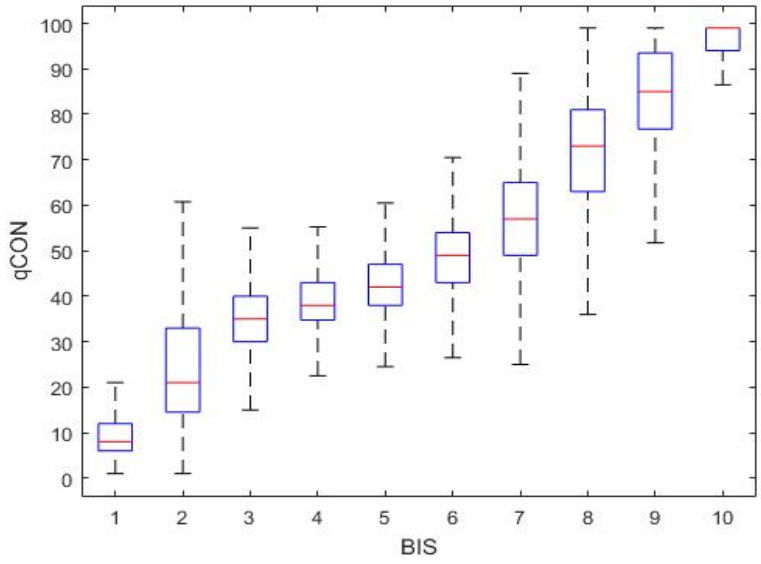

Figure 1: *Boxplot of qCON index with respect to BIS (divided in ten levels)*

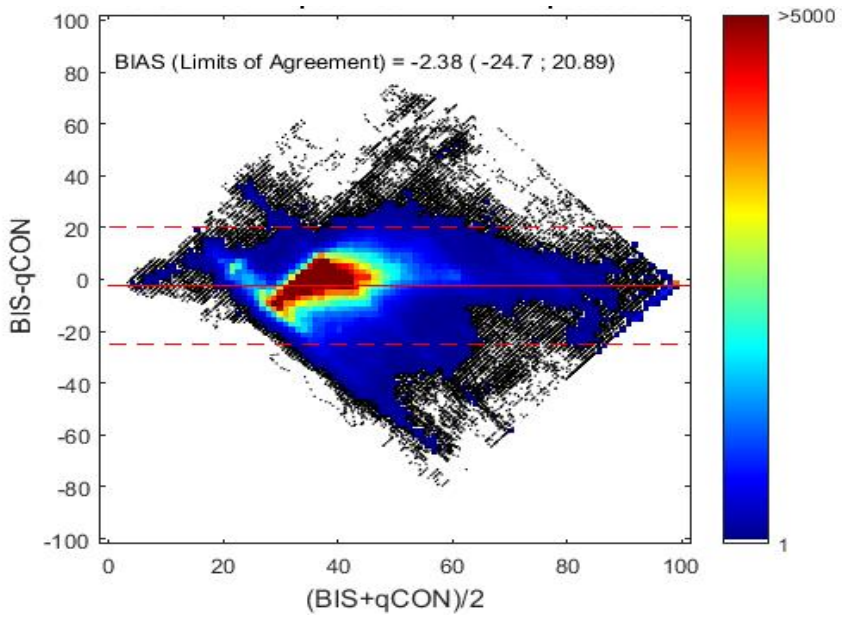

Figure 2: *Bland Altman of BIS and qCON indices.*

Table 1: values of qCON and BIS index before and after the LOC (state of patient):

	Before LOC Mean ± SD	**After LOC Mean ± SD**	**Pk ± SE**
qCON	84.22 ± 12.14	47.70 ± 11.68	0.970 ± 0.005.
BIS	84.16 ± 10.04	46.52 ± 12.17	0.982 ± 0.004

References

[1] Jensen EW, Valencia JF, López A, Anglada T, Agustı´ M, Ramos Y, Gambús P. Monitoring hypnotic effect and nociception with two EEG-derived indices, qCON and qNOX, during general anaesthesia. Acta Anaesthesiol Scand. 2014;58(8):933–41.

[2] Schnider TW, Minto CF, Shafer SL, Gambus PL, Andresen C, Goodale DB, Youngs EJ. The influence of age on propofol pharmacodynamics. Anesthesiology. 1999;90:1502–16.

[3] Minto CF, Schnider TW, Egan TD, Youngs E, Lemmens HJ, Gambus PL, Billard V, Hoke JF, Moore KH, Hermann DJ, Muir KT, Mandema JW, Shafer SL. Influence of age and gender on the pharmacokinetics and pharmacodynamics of remifentanil: I model development. Anesthesiology. 1997;86:10–23.

Do Complexity Measures of Frontal EEG Distinguish Loss of Consciousness in Geriatric Patients Under Anesthesia?

Presenting Author: Sarah L. Eagleman[1*]
Co-Authors: Don A. Vaughn[2,3], David R. Drover[1], Caitlin M. Drover[4], Mark S. Cohen[2,5], Nicholas T. Ouellette[6], and M. Bruce MacIver[1]

[1]Department of Anesthesiology, Perioperative and Pain Medicine, Stanford University, Palo Alto, CA, USA
[2]UCLA Semel Institute for Neuroscience and Human Behavior, Los Angeles, CA, USA
[3]University of Santa Clara, Santa Clara, CA, USA
[4]University of Washington, Seattle, WA, USA
[5]UCLA Departments of Psychiatry, Neurology, Radiology, Psychology, Biomedical Physics, and Bioengineering, and California Nanosystems Institute, Los Angeles, CA, USA
[6]Department of Civil and Environmental Engineering, Stanford University, Stanford, CA., USA

Background / Introduction: While geriatric patients have a high likelihood of requiring anesthesia, they carry an increased risk for adverse cognitive outcomes from its use. Previous work suggests this could be mitigated by better intraoperative monitoring using indexes defined by several processed electroencephalogram (EEG) measures. Unfortunately, inconsistencies between patients and anesthetic agents in current analysis techniques have limited the adoption of EEG as standard of care. In attempts to identify new analyses that discriminate clinically-relevant anesthesia timepoints, we tested $1/f$ frequency scaling as well as measures of complexity from nonlinear dynamics.

Methods: We tested whether analyses that characterize time-delayed embeddings, correlation dimension, phase-space geometric analysis, and multiscale entropy capture loss-of-consciousness changes in EEG activity. We performed these analyses retrospectively on EEG activity collected from a traditionally hard-to-monitor patient population: geriatric patients on beta-adrenergic blockade who were anesthetized using a combination of fentanyl and propofol. We compared these analyses to traditional frequency-derived measures to test how well they discriminated EEG states before and after loss of response to verbal stimuli.

Results: We found spectral changes similar to those reported previously during loss of response. We also found significant changes in 1/*f* frequency scaling. Additionally, we found that our phase-space geometric characterization of time-delayed embeddings showed significant differences before and after loss of response, as did multiscale entropy.

Conclusions: Our results suggest that subtle transitions in EEG activity around loss of consciousness transitions in geriatric patient monitoring can be distinguished with the application of new spectral analyses and complexity analyses from nonlinear dynamics.

Plasma Pharmacokinetics of THC, 11-OH-THC, and THCCOOH

Presenting Author: Thomas K. Henthorn[1,]

Co-Authors: Cristina Sempio[1], Cinnamon Bidwell[3], Marilyn Huestis[4], Uwe Christians[1], Jost Klawitter[1], Susan Mikulich-Gilbertson[2]

[1]Anesthesiology and [2]Psychiatry, University of Colorado, Aurora, CO; [3]Institute of Cognitive Science, University of Colorado, Boulder, CO; [4]The Lambert Center for the Study of Medicinal Cannabis and Hemp, Thomas Jefferson University, Philadelphia, PA

Introduction/Background: Population pharmacokinetic (popPK) modeling of THC, but not including those of the major metabolites, has been performed in a clinical research setting with dense plasma sampling following a closely monitored administration by smoking and vaping.[1] To interpret sparse, observational plasma THC and metabolite concentrations, we aimed to develop a comprehensive popPK model of THC and its metabolites as a Bayesian prior for further modeling of sparse, observational data. We postulated that such a model could estimate daily THC exposure in a cohort of regular cannabis users in Boulder, Colorado.

Methods: Six sequestered subjects smoked in a rigorously-paced manner two different concentrations of marijuana cigarettes (1.75% and 3.55% THC) over 10 min one week apart. Frequent blood samples were obtained during and immediately after each smoking event and then less frequently for one week for the measurement of THC, 11-OH-THC and THCCOOH by LC-MS/MS.[2] A multicompartment popPK model was developed using non-linear mixed effects analysis. 16 regular users of cannabis were recruited into a larger study involving psychomotor testing. Blood samples were obtained at recruitment, in a mobile lab immediately before smoking in their home, upon returning to the mobile lab and then again one hour later for analysis of THC/metabolites. These data were analyzed with the prior, dense data and the Bayesian prior for popPK analysis, including estimates of (1) daily THC consumption prior to recruitment, (2) daily THC consumption in the interval between recruitment and home-smoking and (3) the dose consumed during the home-smoking event.

Results: A 3-compartment PK model of THC was developed (Vss=22.6 L/kg, and Cle=1.12 L/min) with extension to metabolite kinetics. Baseline daily THC consumption was estimated to be 2.56$\pm$3.27 (mean$\pm$SD) NIDA cannabis cigarettes (5.6% THC). Consumption dropped to 0.87$\pm$0.97 cigarettes in the interval prior to home-smoking and 0.45$\pm$0.26 while in their home that was estimated to have begun 14 minutes prior to returning to the mobile lab.

Conclusions: The current study demonstrates the feasibility of developing a popPK model from THC clinical trial studies which when combined with observation plasma THC (and metabolite) data can estimate dose, timing of dose until first blood sample and daily THC consumption.

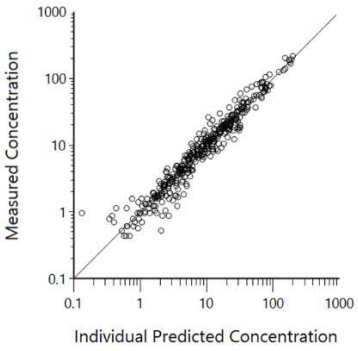

THC

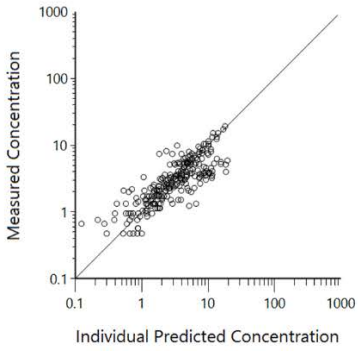

11-OH-THC

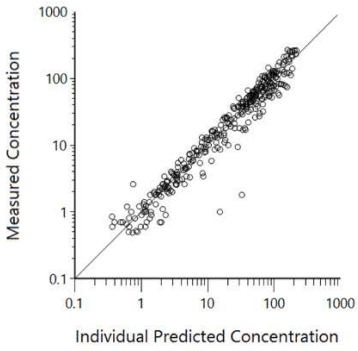

THCCOOH

$GABA_A$ actions of ABP-700 and its Carboxylic Acid Metabolite CPM-Acid: Implications for Toxicological Studies and Clinical Development

Presenting Author: Beatrijs. I. Valk, B.Sc.[1,2]

Co-authors: Megan L. McGrath, B.Sc.[2], Douglas E. Raines, M.D.[2]
[1]University of Groningen, University Medical Center Groningen, Department of Anesthesiology, Groningen, The Netherlands

[2]Department of Anesthesia, Critical Care and, Pain Medicine, Massachusetts General Hospital, Boston, Massachusetts

Background: ABP-700 (also known as cyclopropyl-methoxycarbonyl metomidate) is a soft analog of etomidate. It acts as a positive allosteric modulator of the γ-aminobutyric acid type A ($GABA_A$) receptor and is rapidly metabolized by non-specific esterases to CPM-acid (CPM-A). In toxicological studies using beagle dogs, convulsive seizures were observed during the final 5 minutes of the ABP-700 infusion or in the minutes to hours afterward. The late timing of the seizures suggests that they were caused by the metabolite, CPM-A. In order to better understand the mechanism of such seizures, the $GABA_A$ receptor pharmacology of ABP-700 and CPM-acid were characterized.

Materials and methods: The concentration-dependent actions of ABP-700 and CPM-acid were defined in oocyte-expressed $\alpha_1\beta_3\gamma_{2L}$ $GABA_A$ receptors using voltage clamp electrophysiology. Potentiation of GABA-mediated currents was characterized by adding increasing concentrations of ABP-700 or CPM-A to an EC_5 GABA concentration (6 μM). Inhibition of GABA-mediated currents was characterized by adding drug to a receptor-saturating GABA concentration (1000 μM). The effect of CPM-A on the GABA concentration-response curve was similarly defined using electrophysiological techniques.

Results: The concentration-response curves defining the impact of ABP-700 and CPM-acid on $GABA_A$ receptor-mediated currents evoked by 6 μM GABA was biphasic, potentiating currents at low (clinically-relevant) concentrations while inhibiting them at very high (toxic) concentrations. The EC_{50} for current potentiation was 2.3 μM for ABP-700 (95% CI, 1.623 to 3.309) and 347 μM for CPM-A (95% CI, 123.9 to 971.7; p=0.0025). The IC_{50}s for current inhibition determined using 1000 μM GABA were 752 μM for ABP-700 (95% CI, 657.7 to 859.3) and 1530 μM for CPM-A (95% CI, 1308 to 1718; p<0.0001). CPM-A (1500 μM) reduced the peak current amplitude produced by high GABA concentrations from 104% to 64% (p<0.0001) without altering the GABA EC_{50} (44 μM versus 45 μM in the absence and presence of CPM-A, respectively; p = 0.9146).

Conclusion: Inhibition of $GABA_A$ receptors is a well-established mechanism for seizure production. Our studies show that CPM-acid non-competitively inhibits $GABA_A$ receptors at the blood concentrations achieved in beagle dogs that received prolonged high dose infusions of ABP-700. This provides a mechanistic explanation for seizures observed in beagle dogs, a dog breed known to have a relatively low seizure threshold. This concentration is ~100x

higher than that reached in human clinical studies of ABP-700, suggesting that this action is not clinically relevant.

Potential for Reduction in Interpatient Variability of Propofol Target Concentrations During Protocol Based Anesthesia

Presenting Author: Thomas W. Schnider[1]
Co-Authors: Miodrag Filipovic[1], Charles F. Minto[2]
[1]Dept. of Anesthesia, Intensive Care, Emergency and Pain Medicine, Kantonsspital, St. Gallen, Switzerland. [2]Dept. of Anaesthesia, North Shore Private Hospital, Sydney, Australia.

Background/Introduction: Pharmacokinetic (PK) model based administration of anesthetics takes into account dosing history and patient characteristics. With target controlled infusion (TCI) using an "ideal" PK model, we expect the target concentration to be unbiased with regard to the patient characteristics, except for those affecting the pharmacodynamic (PD) sensitivity to the drug. We therefore assessed the potential to develop a "more accurate" PK model in a real world setting by relating the observed interpatient variability in required propofol target concentrations to patient characteristics using linear regression.

Methods: Setting: Tertiary care hospital with all surgical specialties except for cardiac surgery. Anesthesia: BIS (Covidien, Inc., Mansfield, MA, USA) guided intravenous (i.v.) anesthesia with propofol TCI, remifentanil TCI and fentanyl. TCI target concentrations and BIS values were all recorded automatically from the Fresnius Kabi Orchestra TCI system (Fresenius Vial, Brezins, France) which was programmed with the PK model published by Schnider et al. and from the BIS Monitor (Covidien) respectively.
Protocol: Fentanyl prior to induction (100–200□g) and at the commencement of surgery. Propofol effect site concentration[1,2] (CeT) titrated to achieve a BIS between 40 and 60. During surgery remifentanil added to compensate for offset of fentanyl effect. Towards end of surgery, propofol administration ceased according to the 70–80% decrement time and remifentanil concentration increased to prevent motor response. After the last suture, remifentanil ceased.
Analysis: Surgical cases lasting less than one hour were excluded. In order to reduce variability due to differences in the anesthetic goal (e.g. sedation), only patients who were intubated were included. The CeT 30 min. after skin incision (which was also at least 30 min. before end of surgery) were considered to be the stable maintenance phase and were used for the analysis.
Statistics: Correlation between CeT and patient characteristics was sought with linear regression. Covariates included; weight, age, gender, height, ASA classification and Charlson co-morbidity index. If a covariate improved the fit by less than 1% it was removed from the model. The confidence interval (CI) of the coefficient of determination was estimated with boot strapping. The statistical software used was R version 3.5 (https://www.R-project.org/). The analysis of these data was approved by the local ethics committee.

Results: 4584 TCI anesthesia cases were used for the analysis. Fig 1. shows the time course of the CeT and BIS values. At 30 min. after skin incision, 99% of all CeT were between 1 mg/l and 4 mg/l. Higher CeT were associated with higher BIS values (fig. 2). The overall variability of CeT was substantial compared to the association with the covariates (fig. 2). The final linear model included weight,

age and gender (CeT~weight+bs(age)+gender, bs(): b-spline). The coefficient of determination was 11% (99% CI: 9% - 14%). That is, of the overall variability only 11% could be explained with these covariates (fig. 3), of which age contributed approximately 7%.

Conclusions: We conclude that a “more accurate” model for effect site TCI than the one used for this study, only has the potential to reduce the interpatient variability of the CeT by at most 11%. During protocol based, BIS guided, propofol TCI anesthesia in 4584 patients, the propofol concentrations required to maintain the BIS between 40 and 60 varied between 1 mg/l and 4 mg/l in 99% of the patients during the stable maintenance phase. Only 11% of this variability could be explained by or is associated with patient characteristics. We note that this includes both PK and PD variability. Age has been shown to affect the sensitivity to propofol.[2] It is not possible to differentiate whether the age-related interpatient variability that we observed is due to the suboptimal inclusion of age in the PK model or whether it is due to the known increasing age-related PD sensitivity to propofol. However, we believe it is likely that a substantial fraction of this age-related 7% is attributable to interpatient PD variability. Therefore, based on this “real world data”[3], it is questionable whether new models based on more data will have appreciable clinical benefit.

References:

1. Schnider TW, Minto CF, Gambus PL, Andresen C, Goodale DB, Shafer SL, et al.: The influence of method of administration and covariates on the pharmacokinetics of propofol in adult volunteers. Anesthesiology 1998; 88:1170–82
2. Schnider TW, Minto CF, Shafer SL, Gambus PL, Andresen C, Goodale DB, et al.: The influence of age on propofol pharmacodynamics. Anesthesiology 1999; 90:1502–16
3. Khosla S, White R, Medina J, Ouwens M, Emmas C, Koder T, et al.: Real world evidence (RWE) - a disruptive innovation or the quiet evolution of medical evidence generation? F1000 Research 2018; 7:

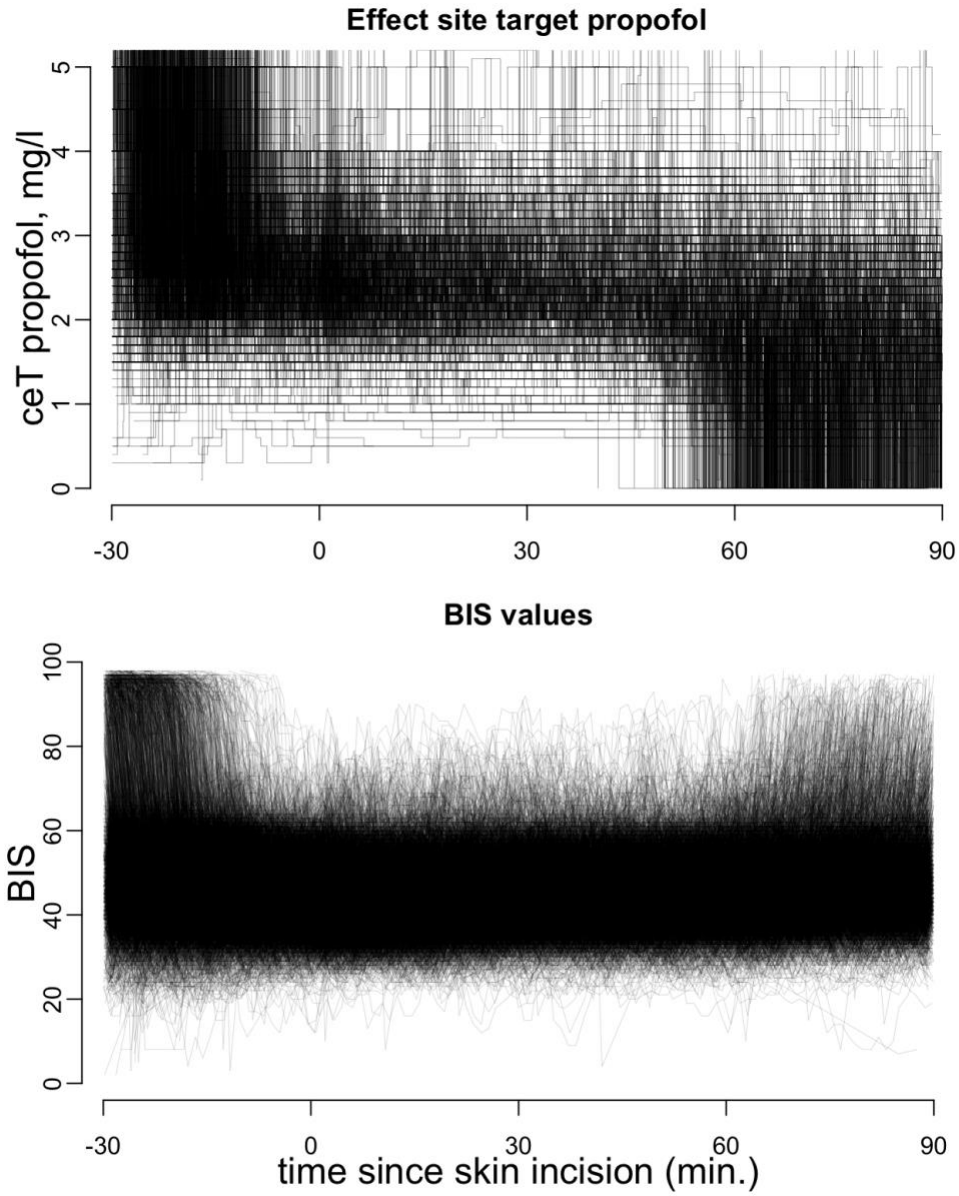

Fig 1:
The raw data of the 4584 patients.

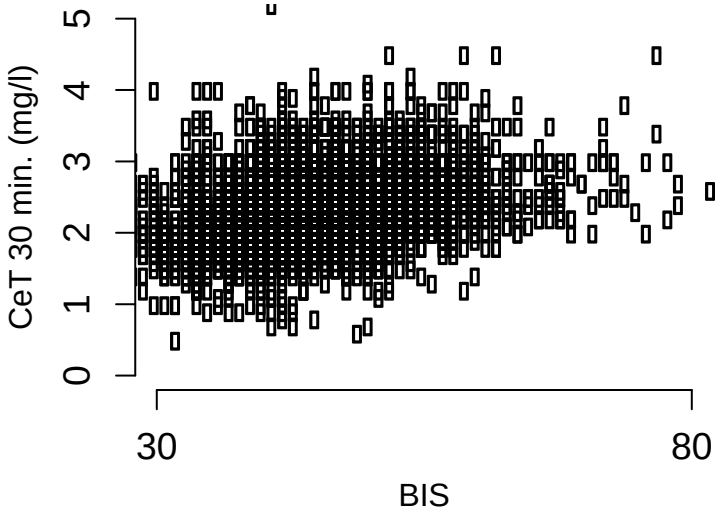

Fig 2.
Higher BIS values were associated with higher CeT. That is, when the PK model is used clinically the CeT is dependent on the BIS unlike during studies where BIS is dependent on CeT.

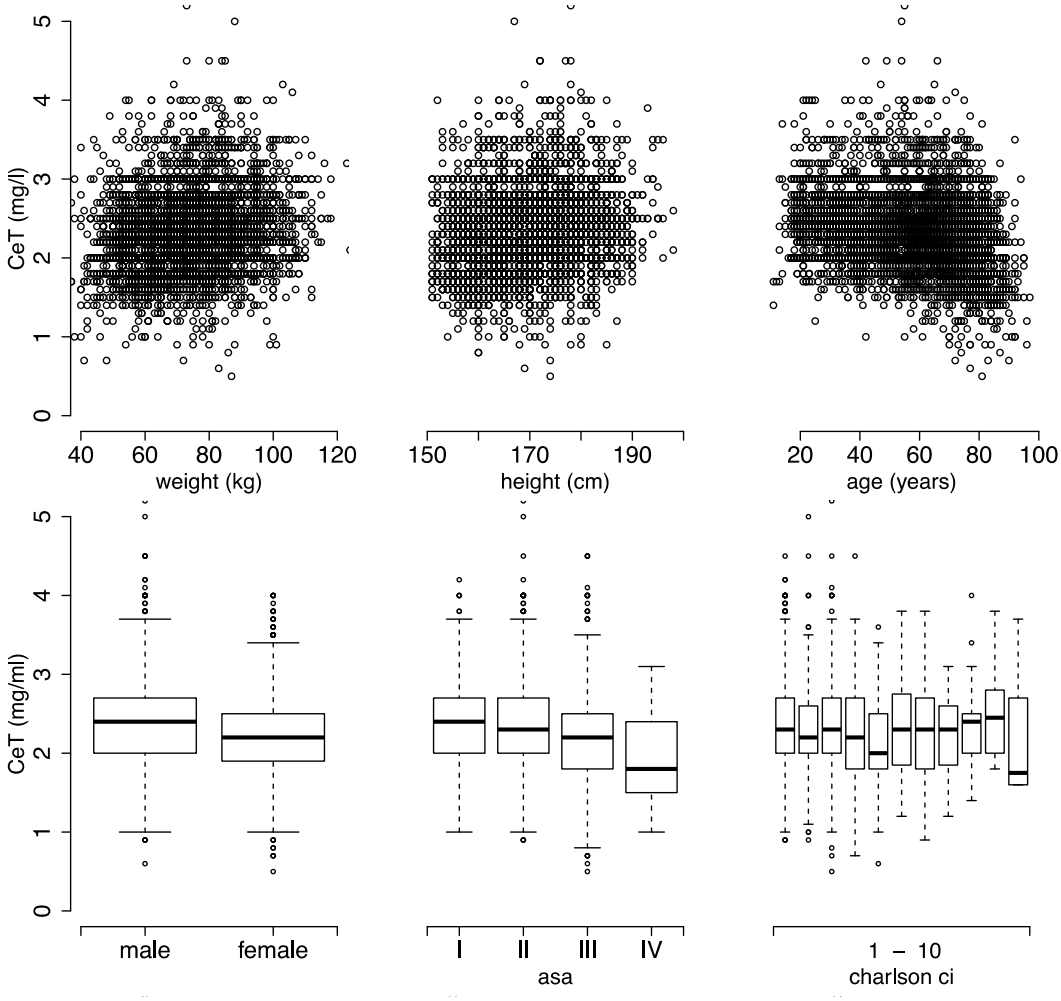

Figure 3.
Plots of the patient characteristics to CeT relationship. Only 11% of the overall interpatient variability was accounted for by covariates. Coefficient of determination from simple linear regression of covariates of the final model: Weight 3.1 %, age 7.7% and gender 2.3%.

.

Modeling Cognitive Function After Deep Sedation Procedures: Nonlinear Mixed Effects Approach

Presenting Author: Pedro L Gambús

First Author: Mireia Alenyà

Co-Authors: Sergio Vide, Iñaki F Trocóniz, Xavier Borrat, Montserrat Vallverdú, Aina Iglesias

Background: Anesthetic drugs used during sedation impair cognitive function (COG-F) even after the sedation procedures have finished. The amount and extent of cognitive impairment has not been adequately explored because objective and fast methods to quantify cognition at the bedside have been lacking. Recently several instruments able to objectively quantify some of the cognitive domains have been commercialized. CogState^{TM} is a software package designed as a battery of psychological tests that can be performed by patients with a laptop in the recovery area. The main objective of this project was to model the dynamics of recovery of cognitive function, measured using CogState^{TM} after sedation-analgesia.

Methods: Under IRB Approval and informed consent 80 patients undergoing deep sedation for gastrointestinal endoscopy in Hospital Clinic of Barcelona were enrolled in the study.
Propofol and remifentanil were administered through Target Controlled Infusion (TCI) system and COG-F was objectively quantified before and at least two more times after the end of sedation. To measure the speed of performance "LMN" the mean of the log10 transformed reaction times for correct responses was used as detection test.
Modeling was performed using a nonlinear mixed effects approach with NONMEM 7.3. Model selection was based on the evaluation of the minimum value of the objective function and goodness of fit plots (GOFs). Visual Predictive Check plots (VPC) and 500-Bootstrap Analysis were performed to evaluate the obtained final model. Covariates evaluated included demographic information, duration and initial hour of sedation procedures and results of Mini-COG test.

Results: The final model selected considers a synergistic interaction between remifentanil and propofol. Parameter values (RSE) were obtained with enough precision: basal LMN value *LMN0* = 2.75 (0.2), slope of the dose-response relationship *SLP* = 94.85 (25), k_{e0PRO} = 2.23 (46) min^{-1}, k_{e0REM} = 1.26 (62) min^{-1} and C_{50P} = 0.55 (6) µg/mL. Significant interindividual variability values (RSE) [SHR] found were *IIV LMN0* = 1.8 (10)[12] and *IIV SLP* = 36 (55)[71].
Age and sex on remifentanil k_{e0} and duration of sedation on basal LMN parameter were the covariates that significantly improved the model.

Conclusions: A population mixed effects model for COG-F recovery after propofol and remifentanil administration has been developed.

Since age, sex and duration of procedures are significant covariates, individualized strategies might be implemented and they should be taken into account when planning a procedure.

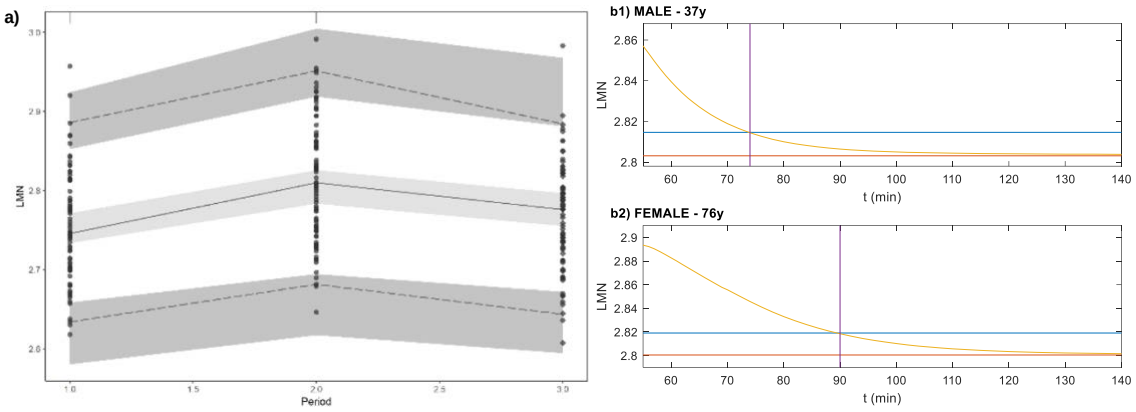

Figure 1. (a) VPC results. Data points represent raw data and lines correspond to its 2.5th, 50th and 97.5th percentiles. Grey shaded areas represent the 95% prediction intervals of the 2.5th, 50th and 97.5th percentiles of 500 simulated datasets. (b) Model simulation results of (b1) a 37y male and (b2) 76y woman. Horizontal red and blue lines show the basal (100%) and the 80% of the LMN value, yellow line corresponds to LMN profile and purple vertical line indicates when LMN curve and 80%LMN line intersect.

Continuous Prediction of Sedation Levels Based on Signal Inputs: Evaluation of Different Modeling Approaches Including Machine Learning

Presenting Author: Pedro L Gambús

First Author: Matthew McDermott

Co-Authors: Sergio Vide, Mireia Alenyà, Iñaki F Trocóniz, Xavier Borrat, Wei-Hu Weng, Peter Szolovits

Background: Monitoring systems are an essential part in diagnosing and therapeutic management of patients, more specially to control and individualize management of patients under anesthesia. Collecting signals that are direct reflect of organs or systems activity allows the clinician to observe in real time how the patient is doing or responding to a treatment. Adequately collected and analysed data from other populations of patients could help in providing more useful information regarding how a patient might respond to a therapy. The present work wants to demonstrate that mathematical models based on prior information from large sets of data can predict level of sedation or probability of side effects in a period of two minutes ahead of time potentially improving monitoring systems with predictive ability.

Methods: Under IRB Approval a new analysis of a database of 380 patients undergoing deep sedation (TCI propofol and remifentanil) for gastrointestinal endoscopy in Hospital Clinic of Barcelona was performed. Hemodynamic variables, raw and processed EEG, transcutaneous pCO2, pulse oximetry as well as drug input were collected every second. Ramsay Sedation Scores (RSS), response to noxious stimulation such as endoscopy tube introduction were also recorded.
Individuals were divided into ten random folds for cross-validated model evaluation under three high-utility tasks: predicting RSS, GAG response, and spontaneous decompensation. Three classes of model were examined: logistic regression models, random forest models, and deep learning models. Models used 21 continuously measured input features, spanning hemodynamic variables, processed EEG signals, pCO2 and SpO2 variables, and drug input, all with missingness. Models optimized a cross-entropy loss and output a probabilistic prediction of the target.

Results: On all tasks, the optimal model outperformed a majority class prediction baseline by a statistically significant ($p \leq 0.05$) margin. For RSS prediction and GAG prediction, L1-regularized logistic regression performed best, yielding accuracies of 59.2 ± 1.0% (chance 36.6 ± 4.9%) and 78.7 ± 2.2% (chance 74.5 ± 4.1%), respectively. On spontaneous decompensation, a random forest model performed best, yielding accuracy 62.5 ± 4.1% (chance 50%). Dataset size is yet too small to allow deep learning approaches to succeed on these tasks, but sufficient for simpler non-linear models (random forests) to offer significant advantages on some tasks.

Conclusions: Machine learning models based solely on the continuous, in-procedure covariates can yield local predictive value in predicting three clinically useful measures: RSS, GAG after endoscopy tube insertion, and spontaneous decompensation. This suggests that increased use of in-procedure machine learning techniques could yield clinical benefits.

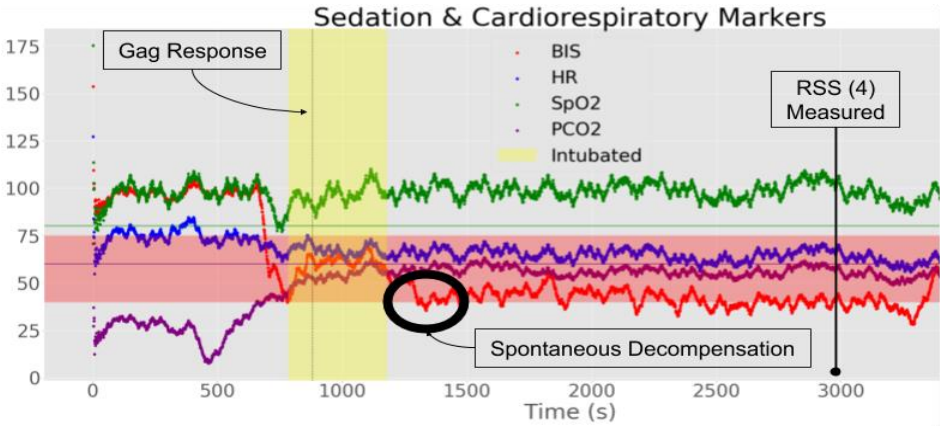

Figure 1. An example of our input data, and prediction target sites.

Anesthetic preconditioning protects *S. cerevisiae* from a lethal heat stress.

Presenting Author: Anita Luethy[1, 2]
Co-Authors: James D. Boghosian[1], Christoph Kindler[2] and Joseph F. Cotten[1]
[1]Department of Anesthesia, Critical Care and Pain Medicine, Massachusetts General Hospital, Boston, USA; [2]Department of Anesthesia, Kantonsspital Aarau, Aarau, Switzerland

Background/Introduction: Anesthetic action and preconditioning are conserved across all living organisms (1, 2). We hypothesize that anesthetics invoke a cellular stress response in yeast protective from an otherwise lethal stress. Establishing *S. cerevisiae* as a model organism for anesthetic preconditioning may allow high throughput screening for more potent, efficacious, and less toxic protective compounds. Additionally, high throughput assays may uncover molecular mechanisms of cellular protection.

Methods: Potency for protection was determined by pretreating *S. cerevisiae* with and without anesthetic compounds at varying temperatures before exposing them to a usually lethal heat stress. Cell viability was detected by optical density measurements and by colony forming unit assays.

Results and Discussion: Anesthetics dose-dependently protect *S. cerevisiae* from a lethal heat stress with the following rank order for potency: CBr4 > Propofol > TBE > HFP > TFE > Isopropanol > Ethanol and TCE > DCE > MCE (Table 1). Potency for protection correlates log-linearly with compound lipophilicity (R square 0.94). CBr4, TBE, TCE and HFP enhance protection induced by mild to moderate temperature elevation.

Conclusions: Anesthetics protect *S. cerevisiae* from a lethal heat stress and enhance protection induced by mild to moderate temperature elevation. *S. cerevisiae* may be a useful organism to characterize pharmacological requirements for anesthetic preconditioning.

References: (1) Sonner JM, Anesthesia and Analgesia 2008 Sept;107(3):849. (2) Jia B, Anesthesiology 2008 Mar;108(3):426-33.

Funding: Massachusetts General Hospital Department of Anesthesia, Critical Care & Pain Medicine; NIH/R01-HL117871; and Kantonsspital Aarau, Aarau, Switzerland (1410.000.062).

Table 1.

Compound	Concentration for maximum Protection ± SEM	n-value	logP
Propofol	310 ± 0µM	3	3.79

Carbon tetrabromide	33.8 ± 2.8µM	9	3.42
2,2,2-tribromoethanol	5.6 ± 0mM	9	2.1
2,2.2-trichloroethanol	31 ± 0mM	6	1.42
1,1,1,3,3,3-hexafluoroisopropanol	19.3 ± 2.8mM	6	1.66
2,2,2-trifluoroethanol	193.3 ± 28.3mM	6	0.41
2,2-dichloroethanol	100 ± 0mM	3	0.43
2-monochloroethanol	310 ± 0mM	3	0.03
Isopropanol	560 ± 0mM	3	0.05
Ethanol	1 ± 0M	3	-0.31

Prediction of the Effect-Site Concentration of Remifentanil Based on the Pupillary Light Reflex

Presenting Author: Sérgio Vide

Co-Author: Pedro Gambús

Department of Anesthesia, Hospital Pedro Hispano

Introduction: The pupillary effects of opioids have been previously studied and described [1,2], in particular its effects on the pupillary reflex dilation (PRD) response and the pupillary unrest under ambient light (PUAL). On the other hand, and although the miotic action of opioids on the pupil is widely known, the dose-response changes of the pupillary light reflex have not been described. The aim of this study was to assess the Pupillary Light Reflex (PLR) association with different concentrations of remifentanil, and the possibility of predicting remifentanil concentrations based on the different parameters of this reflex.

Methods: Preliminary data from an observational prospective study was used, and 6 patients were included. They were scheduled for ambulatory procedures under sedation. Remifentanil was administered using a TCI pump from Fresenius Base Primea docking station (Fresenius - Kabi, Germany) using Minto PK-PD Model. Before starting, and at each target concentration after equilibration between plasmatic and biophase, the PLR was measured using a portable infrared pupillometer (AlgiScan® - IDMed, France). The pupillometer applied a flash of visible light and measured the initial diameter, the minimum diameter obtained afterwards, the response latency and velocity of contraction. These variables were then analyzed in the IBM SPSS Modeler software.

Results: A total of 22 measurements of PLR were obtained with concentrations ranging from 0 to 4 ng/mL. The model presenting best accuracy was a Bayesian network (figure 1), with an accuracy of 81,8% (figure 2).

Conclusions: These preliminary results suggest that is possible to predict the effect site concentration of remifentanil based on the PLR. This also shows that the PLR changes in a dose-dependent manner with remifentanil. Based on these results, it might be possible to establish equipotency relationships among opioids using the PLR. However, further data is needed to enhance this model.

References:

1. Neice AE, Behrends M, Bokoch MP, Seligman KM, Conrad NM, Larson MD. Prediction of Opioid Analgesic Efficacy by Measurement of Pupillary Unrest. *Anesth Analg*. 2017;124(3):915-921. doi:10.1213/ANE.0000000000001728

2. Larson MD. Mechanism of opioid-induced pupillary effects. *Clin Neurophysiol*. 2008;119(6):1358-1364. doi:10.1016/j.clinph.2008.01.106

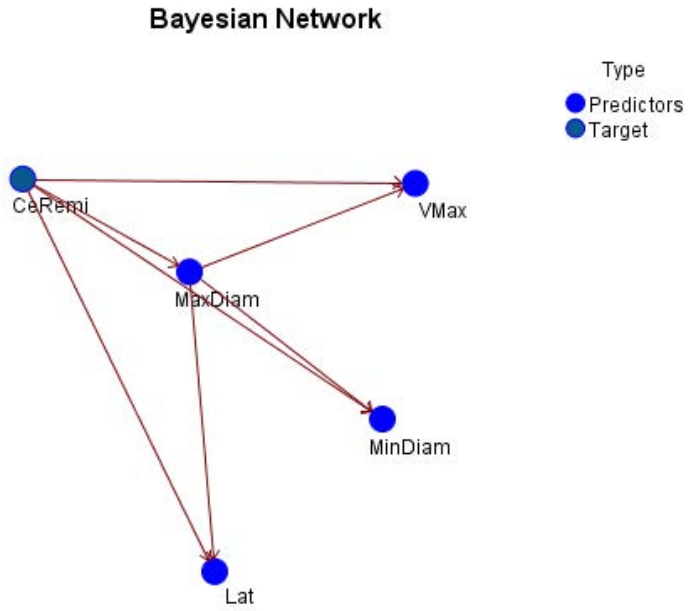

Figure 1 - Illustration of the Bayesian network used

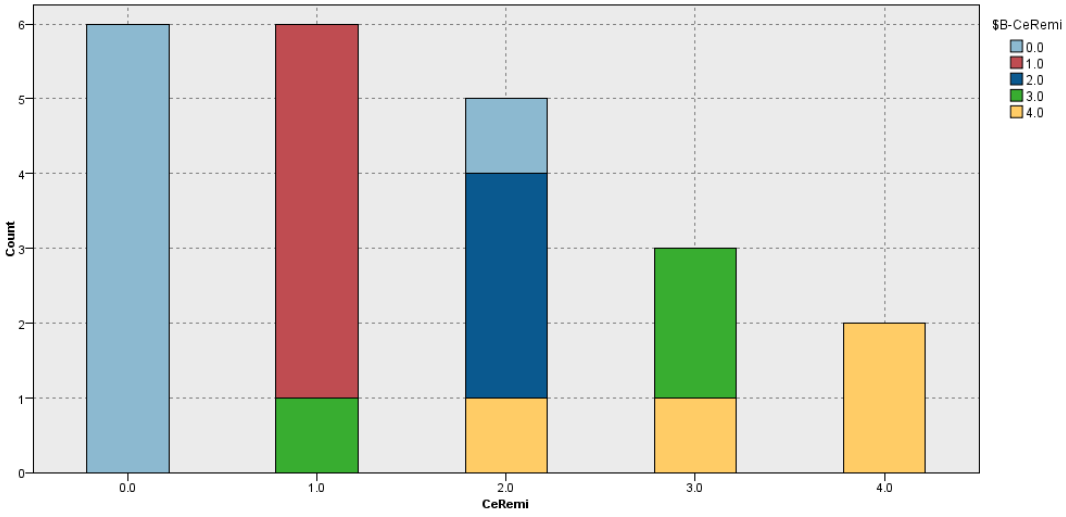

Figure 2 - Accuracy of the predictions for each Remifentanil effect site concentration

Pain on *IV* Cannulation or After a Small Dose of Propofol do Not Predict Postoperative Opioid Requirements

Presenting Author: Ross Kennedy[1,2]
Co-Authors: Rachel Matthews[1,2], Margie McKellow[1]

[1]Department of Anaesthesia, Christchurch Hospital
[2]University of Otago: Christchurch
Christchurch, New Zealand

In an effort to optimise post-operative analgesia we have used calculated effect site fentanyl concentrations (Ce-fent) as a marker of opioid requirement to explore the relationship between intraoperative opioid dosing and post-operative requirements. A recent study {Persson:2015ki} described an association between pain on injection of a small dose of propofol and morphine requirements in PACU.

The aim of this study was to explore the relationship between the response to a preoperative noxious stimulus and PACU Ce-fent.

Methods: NZ HDEC Ethics review. Subjects were ASA 1-3 patients booked for elective laparoscopic surgery. IV cannula inserted and 3ml propofol administered. Pain after iv insertion and after propofol recorded using a 100mm visual analogue scale and the maximum taken as the preoperative value. Conduct of anaesthesia at discretion of primary clinician, with fentanyl as only opioid used. All drug doses in the OR and PACU recorded and Ce-fent calculated over time. In PACU pain scores recorded along with time to first analgesia. We extracted Ce-fent at various time points, including on reaching PACU discharge criteria. Correlations were explored using the slope of the best fit linear regression line.

Results: 60 subjects recruited. 49F, 11M. 40 undergoing a range of laparoscopic gynaecological surgery. 14 ASA1, 29 ASA 2, 9 ASA 3. Mean (SD) age 50.5 (17.4)yr, BMI 28.2 (6.2) $kg.m^{-2}$.
Highest preop VAS was (median [quartiles]) 27 [9, 51]. Mean intraoperative Ce-fent 1.4 [1.1, 1.6] ng/ml. Ce-fent on PACU arrival 0.84 [0.64, 1.07] ng/ml. Time to first opioid in PACU 27 [15, 51] min. Highest PACU pain VAS 52 [22, 70]. Discharge Ce-fent 0.76 [0.57, 0.93] ng/ml.

We found no correlation between the highest preoperative VAS and time to first opioid in PACU (95%CI of regression line slope -0.19 to 0.39), highest PACU VAS (-0.014 to 0.643) or Ce-fent at PACU discharge (-0.0018 to 0.0034).

There was no difference in PACU discharge Ce-fent or highest PACU VAS pain scores between subjects in the upper quartile of preop VAS and the remainder of subjects. (Mann-Witney test p=0.17 and p=0.34 respectively)

We did find an association between mean intraoperative Ce-fent and PACU discharge Ce-fent (95%CI slope 0.13 to 0.42).

Discussion: In this small study we were unable to demonstrate that pain on iv cannulation or on injection of a small dose of propofol reliably predicts postoperative analgesic requirements. As previously, we found a correlation between intraoperative and PACU Ce-fent.

Sevoflurane Consumption at Different Stages of Paediatric Anaesthesia – an Observational Audit

Presenting Author: Ross Kennedy[1,2]
Co-Authors: Benjamin van der Griend[1]

[1]Department of Anaesthesia, Christchurch Hospital
[2]University of Otago: Christchurch
Christchurch, New Zealand

We are interested in patterns of volatile anesthetic use so that we can work to minimise wastage (1). The cost saving and environmental implications of reducing unnecessary volatile use is well recognised. We previously reported (2) that short pediatric ORL cases, using inhalational induction used as much sevoflurane as major abdominal operations in adults lasting four times as long. We now wish to gain a better understanding of the pattern of use of inhalational anesthetics in our paediatric patients.

Methods: This study was approved by the New Zealand HEDC. We observed all cases occurring during normal working hours in patients <=16yr in a single OR dedicated to paediatric surgery over an eight week period. This OR has an induction room with a GE-Avance machine and a GE-Aisys in the OR itself. In our hospital all adults are induced in the OR. We recorded basic demographics, timings, breathing circuit and airways used along with sevoflurane consumption taken from the logs of the machines. Patients not receiving sevoflurane for maintenance of anesthesia were excluded.

Results: We collected data from 111 cases, 18 were excluded leaving 94 cases for analysis. Data are presented in the tables.
In essence, children receiving inhalational induction were younger and, on average, lighter than those having an iv induction. Cases utilising an inhalational induction consumed twice as much sevoflurane as those with an iv induction (median 22 [quartiles 16, 26]ml *vs* 11 [7, 17] ml, p<0.00001) although the duration of anesthesia was similar in the groups (49 [35, 17] min *vs* 57 [33-79]min, p=0.79) and sevoflurane usage during the maintenance phase was similar. The use of the induction room and a second machine did not affect sevoflurane consumption.

Discussion: There is increasing awareness of the financial and environmental cost of the wastage of volatile anesthetics. In this study we found that use of inhalational induction doubles the amount of sevoflurane used. This parallels our data in adults which suggests that although gas flow rates during the maintenance phase are an important determinant of overall vapor use, the induction period can have a significant effect on overall consumption.
The next stage is to understand the patterns of FGF & vapor settings used by anesthesiologists in our department during inhalational induction to look for ways this procedure can be modified without impairing the clinical utility of this procedure.

References:

1. Kennedy, R., French, R., Vesto, G., & Hanrahan, J. (2017). Gas flows during induction have a major effect on overall vapor consumption despite low

maintenance flows. *Proceedings of the American Society of Anesthesiologists (ASA) Anesthesiology Annual Meeting.* A3039.

2. Kennedy, R., van der Griend, B., Page, J., Vesto, G., & French, R. (2017). Brief pediatric cases use a similar mass of sevoflurane as adult anesthetics lasting over an hour. *Proceedings of the International Society for Anaesthetic Pharmacology (ISAP) Annual Meeting.* (pp. 24).

Table 1: Patient Age and Weight of Included Cases

	Total n=94	Gas induction n=65	IV induction n=29	*p* (Mann Whitney)
Median Age (years)	4 (IQR=2-6.75)	3 (IQR=1-5)	6 (IQR=4-11)	<0.001
Median Weight (kg)	16 (IQR=12-26)	15 (IQR=10-21)	24 (IQR=16-40)	0.002

Table 2: Median Liquid Sevoflurane Consumption (mL)

	Total n=94	Gas induction n=65	IV induction n=29	*p* (Mann Whitney)
Sevoflurane total	19 (IQR=13-24)	22 (IQR=16-26)	11 (IQR=7-17)	<0.00001
Induction Phase*	12 (IQR=6.5-16)	13.5 (IQR=11-18)	4 (IQR=1-7)	<0.00001
Maintenance	7 (IQR=5-10)	7 (IQR 4.75-10)	8 (IQR=6.75-10)	0.53

*Induction Phase is defined as the time from the commencement of anesthesia until the patient was ready for positioning for surgery.

Opioid Use, Gene Expression and Gene Variants Involved in Pain, Inflammation and Dependency Pathways

Presenting Author: Ken B. Johnson
Co-Authors: Alan R. Light, Daniel W. Odell, Ami R. Stuart, Kathleen C. Light

Department of Anesthesiology, University of Utah, Salt Lake City, UT, USA

Background/Introduction: Opioid consumption may influence gene expression of proteins associated with pain transmission and inflammation. With the development of mRNA sequencing tools, investigators have measured gene expression of proteins involved in pain transmission. One aim of this preliminary study was to compare mRNA expression of proteins in opioid consuming and opioid naïve patients before and after surgery. We focused on genes that might alter microglia activation. Recent work has implicated opioids as an activator of microglial cells via an increase in the expression of pro-inflammatory cytokines and components of the complement cascade. Our hypothesis was that gene expression of selected complement cascade proteins would be different in these patient groups before and/or 24 hours after surgery for lower extremity total joint replacement.

Gene variants may also contribute to how patients experience perioperative pain. A second aim was to explore differences in single nucleotide polymorphisms (SNPs) of genes in drug metabolism, GABA, and prostaglandin pathways between opioid naïve and consuming patients. Only those SNPs with moderate to deleterious impact were considered. Our hypothesis was that opioid consuming patients would have more SNPs than opioid naïve patients.

Methods: In a convenience sample of 20 patients undergoing elective lower extremity total joint replacement, ASA class I-III, with 48+ hour hospital stay, we compared genes associated with pain and inflammation in patients that consumed opioids (3-120 mg of oral morphine equivalents per day, n= 11) to those that did not (n=9) for differential expression. WBCs were assayed for mRNA expression of complement proteins and gene variants in drug metabolism, GABA, and prostaglandin pathways.

Results: The gene expression of a complement inhibitor, C4BPA, was reduced and the expression of a complement activator, CFD, was increased in opioid consuming patients (Figure 1). Gene variants in drug metabolism, GABA, and prostaglandin pathways were more common in opioid consumers (average number of variants = 2.45) than in opioid naive patients (average number of variants = 0.67, Table 1).

Conclusions: This preliminary work suggest opioid consuming patients may have genetic susceptibility to altered pain and inflammatory responses and altered expression of inflammation pathways. Additional work is warranted to confirm these findings.

Acknowledgements: The authors wish to thank Timothy J. Parnell, PhD, Associate Director, Bioinformatics Core, Huntsman Cancer Institute, Salt Lake City, Utah for his expertise in analyzing the mRNA sequencing data.

Figure 1

Figure 1A

Figure 1B

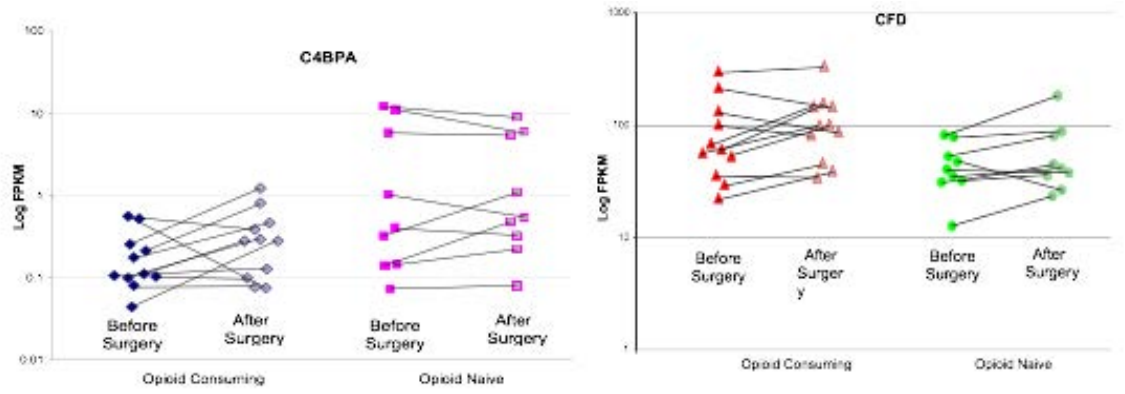

Figure 1. White blood cell messenger RNA Fragments Per Kilobase Million mapped reads (FPKM) for Complement 4 Binding Protein (C4BPA) in opioid consuming (diamonds) and opioid naïve patients (squares, Figure 1A) and FPKM for Complement Factor D (CFD) in opioid consuming (triangles) and opioid naïve patients (circles, Figure 1B) before and 24 hours after surgery. In RNA-Seq, the relative expression of a transcript is proportional to the number of cDNA fragments that originate from it. Data are from each of the 20 individual patients. The before and after surgery values for the same patient are linked (black lines). FPKM values are presented on a log scale (base 10).

Table 1. Gene Variants in Opioid Naïve and Consuming Patients

Opioid Consuming Patients (n=11, mean number of variants= 2.45)

ID	Drug Metabolism Variants			Prostaglandin Variants		GABA Variants	Total
1							0 variants
4	CYP1B1			PTGES2			2 variants
8	CYP1B1			PTGES2		DBI	3 variants
10	CYP1B1						1 variant
12	CYP1B1			PTGES2	PTGS1		3 variants
13	CYP1B1				PTGS1		2 variants
14	CYP1B1			PTGES2			2 variants
15	CYP1B1	AHR	AKR1A1			DBI	4 variants
16	CYP1B1	AHR	AKR1A1				3 variants
17	CYP1B1			PTGES2		DBI	3 variants
19	CYP1B1	AHR	AKR1A1		PTGS1		4 variants

Opioid Naive Patients (n=9, mean number of variants= 0.67)

2							0 variant
3				PTGES2			1 variant
5	CYP1B1		AKR1A1				2 variants
6							0 variant
7	CYP1B1						1 variant
9							0 variant
11							0 variant
18	CYP1B1						1 variant
20	CYP1B1						1 variant

CYP1B1: Cytochrome P450 Family 1 Subfamily B Member 1, monooxygenases which catalyze many reactions involved in drug metabolism and synthesis of cholesterol, steroids and other lipids.
AHR: Aryl Hydrocarbon Receptor, regulates metabolizing enzymes such as cytochrome P450.
AKR1A1: Aldo-Keto Reductase Family 1 Member A1, participates in both the drug metabolism and prostaglandin pathways.
PTGES2: Prostaglandin E Synthase 2, catalyzes the conversion of prostaglandin H2 to prostaglandin E2
PTGES1: Prostaglandin-Endoperoxide Synthase 1, catalyzes the conversion of arachinodate to prostaglandin.
DBI: Diazepam Binding Inhibitor, involved in lipid metabolism and the displacement of beta-carbolines and benzodiazepines, which modulate signal transduction at type A gamma-aminobutyric acid receptors located in brain synapses.
Source: https://www.genecards.org/

Hypnotic/opioid Interactions and Response to Noxious Stimulations during Peripheral Urological Procedures Assessed through the SMART Pilot View™ (SPV)

Presenting Author: Frederique Servin[1]
Co-Authors: Laetitia Desplanque[1], Philippe Montravers[1]

[1] APHP Hôpital Bichat Claude Bernard, HUPNVS, Paris, France

Background/Introduction: During general anesthesia (GA), control over the response to nociceptive stimulations results from the synergy between hypnotics and opioids. The Smart Pilot View™ (Dräger, Germany) (SVP) displays the hypnotic/opioid interaction and calculates an index (NSRI) based on the predicted or measured concentrations of the agents to quantify its magnitude (1). Currently, the value of this index in relation to the level of surgical stimulation remains mostly unknown, as well as its inter-individual variability.

This study was designed to assess the value of NSRI associated with an adequate control over anesthesia during peripheral urological procedures and to describe the relationship between age, NSRI and predicted effect site concentrations of anesthetic agents.

Methods: The data recorded from the SPV of all adult patients undergoing peripheral urological procedures (prostatic or bladder resections, laser removal of stones) under GA using propofol and remifentanil between September 2017 and February 2018 were retrospectively analyzed. These data include date and time of surgery, characteristics of the patient (age, gender, weight, height), bispectral index (BIS), mean arterial pressure, predicted effect site concentrations of propofol (CeP) and remifentanil (CeR), and calculated NSRI. The actual name of the patient was not recorded.

Only the periods during which the anesthesia level was adequate (BIS between 40 and 60 and MAP ± 30% of the baseline value) were analyzed.

The results are expressed as mean ± standard deviation.

The relationship between age, anesthetic agents and NSRI was described by linear regression and correlation analysis.

Results: 73 patients were included: M/F 59/14; mean age 62 ± 15 yrs; duration of the procedure 61± 27 min (greenlight laser 20; laser fragmentation of stones 18; transurethral bladder resection 13; installation of a double J catheter 6 …).

During the periods of adequate anesthesia, the BIS value was 50 ± 6 and the MAP was 86 ± 14 mmHg.

The mean CeP was 2.46 ± 0.72 mcg/mL. There was a weak, non-statistically significant inverse correlation between age and CeP (cor = 4.47%, p = 0.072). The mean CeR was 3.11 ± 1.00 ng/mL. No correlation could be found between age and

CeR (cor = 0.6%, p = 0.58). The mean NSRI was 49.3 ± 17.3. There was a significant correlation between age and NSRI (cor = 8.15%, p = 0.014).

Conclusion: For peripheral urological procedures performed under GA associating propofol remifentanil and a laryngeal mask, the NSRI associated with adequate anesthesia levels is around 50. The correlation between NSRI and age was weak, but better than that between either CeP or CeR and age. With increasing age, the NSRI required to ensure adequate anesthesia levels tends to increase.

Further studies will need to assess whether NSRI remains in the same order of magnitude with volatile hypnotic agents rather than propofol, and the influence of different levels of surgical stimulation on the NSRI.

Reference:

1) Anesthesiology. 2010 Apr;112(4):872-80